Ocean Sci., 21, 283–323, 2025
https://doi.org/10.5194/os-21-283-2025

Ocean Science Open Access EGU

Blending 2D topography images from the Surface Water and Ocean Topography (SWOT) mission into the altimeter constellation with the Level-3 multi-mission Data Unification and Altimeter Combination System (DUACS)

Gerald Dibarboure[1], Cécile Anadon[2], Frédéric Briol[2], Emeline Cadier[2], Robin Chevrier[2], Antoine Delepoulle[2], Yannice Faugère[1], Alice Laloue[2], Rosemary Morrow[3], Nicolas Picot[1], Pierre Prandi[2], Marie-Isabelle Pujol[2], Matthias Raynal[1], Anaelle Tréboutte[2], and Clément Ubelmann[4]

[1]Centre National d'Etudes Spatiale (CNES), Toulouse, France
[2]Collecte Localisation Satellites (CLS), Ramonville-Saint-Agne, France
[3]Laboratoire d'Etudes en Géophysique et Océanographie Spatiales (LEGOS), Toulouse, France
[4]Datlas, Grenoble, France

Correspondence: Gerald Dibarboure (gerald.dibarboure@cnes.fr)

Received: 20 May 2024 – Discussion started: 27 May 2024
Revised: 9 October 2024 – Accepted: 28 October 2024 – Published: 30 January 2025

Abstract. The Surface Water and Ocean Topography (SWOT) mission delivers unprecedented swath-altimetry products. Despite SWOT's 2D coverage and precision, its Level-2 ocean products suffer from the same limitations as their counterparts from nadir altimetry missions. To achieve the mission's primary science objectives, the space agencies generate Level-2 ocean products with SWOT alone. In contrast, some research domains and applications require consistent multi-mission observations, such as the Level-3 ocean products provided by the Data Unification and Altimeter Combination System (DUACS) for almost 3 decades and with 20 different satellites. In this paper, we describe how we extended the Level-3 algorithms to handle SWOT's unique swath-altimeter data. We also illustrate and discuss the benefits, relevance, and limitations of Level-3 swath-altimeter products for various research domains.

1 Introduction

The Surface Water and Ocean Topography (SWOT) satellite is an international collaboration between the National Aeronautics and Space Administration (NASA, United States of America), the Centre National d'Etudes Spatiales (CNES, France), the Canadian Space Agency (CSA), and the United Kingdom Space Agency (UKSA). The mission's objective is to make the first global survey of Earth's surface water: ocean surface topography, inland water heights, and river discharge. Morrow et al. (2019) or Fu and Rodriguez (2004) detail the mission's goals, and Fu et al. (2024) illustrate the breakthrough provided by SWOT during its first months of operation.

To achieve this goal, the main instrument of the SWOT mission is a Ka-band interferometer (KaRIn) that delivers a two-dimensional (2D) view of the water surface topography (Peral et al., 2024). To meet its requirements, the interferometer requires an extremely precise attitude and orbit control system (AOCS), as well as the full suite of a "conventional" altimetry payload: a nadir altimeter (Positioning Ocean Solid Earth Ice Dynamics Orbiting Navigator (POSEIDON-3C), Jason-class), precise orbit determination sensors (Détermination d'Orbite et Radiopositionnement Intégré par Satellite (DORIS) positioning system, precise Global Navigation Satellite System, laser reflector array), and a microwave radiometer (to correct for the wet-troposphere path delay). SWOT was first operated on a 1 d repeat orbit from April to July 2023 during the calibration and validation phase (or fast-repeat phase). During this phase, it provided not only the first 2D water surface topography over all water surfaces

(ocean, rivers, and lakes and sea and land ice) but also the first daily revisit of surface water topography by any satellite altimeter mission. Then, by the end of July 2023, the satellite was moved to its science orbit, where it provides global coverage up to a latitude of 78° with an exact repeat of 21 d (Lamy and Albouys, 2014).

SWOT has various product levels that follow the classical conventions from radar altimetry. Firstly, Level 0 (L0) is the reconstructed, unprocessed instrument and payload telemetry data at full resolution. Level 1B (L1B) is the Level-0 data, processed to sensor units and corrected for instrumental and geometrical effects (e.g., calibrated altimeter waveform or KaRIn interferogram). Level 2 (L2) is the Level-1 data transformed into geophysical units and corrected for environmental effects. Level 3 (L3) is a multi-sensor, calibrated (e.g., using a reference altimeter), and simplified product. Lastly, Level 4 (L4) is a multi-mission product where all datasets are mapped on uniform space–time grid scales.

The two important SWOT features over the ocean are its ability to provide a synoptic 2D view of the ocean surface without interpolation and its precision (millimeter-scale noise). When combined, these assets make it possible to capture many ocean features, such as small mesoscale or internal waves as small as a few kilometers. This is a massive improvement in resolution when compared with pre-SWOT images combined from multiple 1D satellites (Fig. 1). Ballarotta et al. (2019) have shown that the effective resolution of pre-SWOT altimetry maps is 200 km or more (in wavelength) and that a significant amount of temporal smoothing (20 d or more) is necessary to assemble such a gridded product from multiple 1D altimetry profiles. In comparison, SWOT's image provides a synoptic and precise view of the mesoscale field for this Gulf Stream region with each revisit: large eddies that were resolved before (Fig. 1a) are consistently captured by SWOT (Fig. 1b). Moreover, they are much better outlined, with stronger anisotropic amplitudes and gradients, and are no longer artificially smoothed in space or in time. SWOT also resolves eddies as small as 10 km in diameter that were never observed in 2D before this mission.

At the time of this writing, the mission's error budget has not been formally published (SWOT, 2024). Nevertheless, preliminary reports such as Raynal et al. (2023), Bohé (2023), Chen (2023), and Fjörtoft (2023) highlight nominal behavior of the first Level-2 products of the SWOT mission. Similarly, Peral et al. (2024) provide an in-depth review of the good behavior of the KaRIn instrument. So in the context of this paper, we will assume that SWOT is meeting its requirements and that Level-2 products are trustworthy and final, although some minor changes might still be implemented by the SWOT project in the coming months.

Nevertheless, the Level-2 products from SWOT suffer from the same limitations as other altimetry missions. Firstly, the processing standards (e.g., geophysical corrections and models) were defined a couple of years before launch, and there is often a significant delay before the complex ground

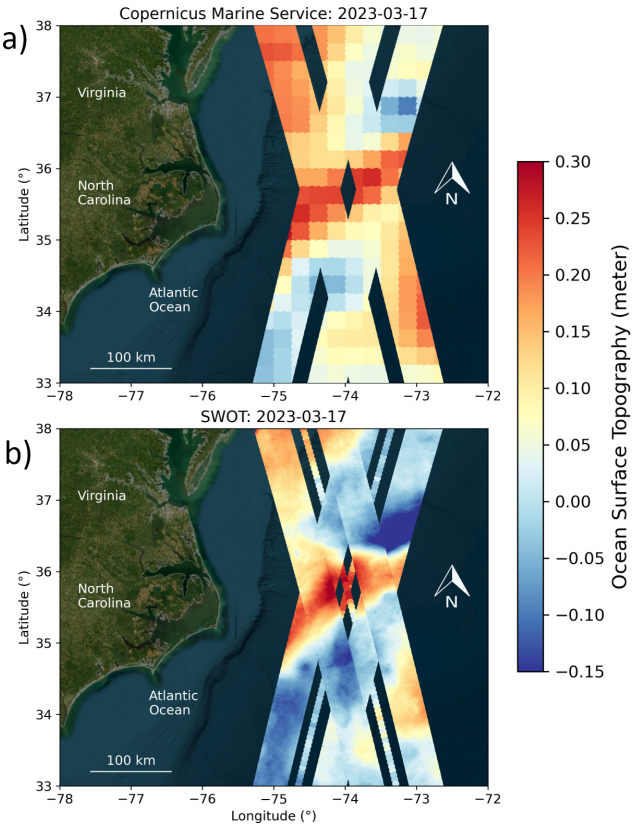

Figure 1. Comparison between 1D and 2D altimetry in the Gulf Stream region. Panel **(a)** is a Level-4 map from 1D nadir altimetry (0.25° product from Copernicus Marine Service based on seven nadir altimeter satellites with no graphical smoothing). Panel **(b)** is our Level-3 product from SWOT in the same region.

segment[1] integrates state-of-the-art upgrades from research papers. Secondly, the L2 ocean products use a complex series of quality flags that do not always match user needs, to say nothing of being consistent with the flagging strategies of other satellites. Thirdly, the SWOT ground segment uses the Level-2 calibration strategy described by Dibarboure et al. (2022). This implementation of a SWOT standalone ground segment is consistent with the mission's hydrology requirements during the science phase, but it was shown to be suboptimal for oceanography, as well as being prone to multi-mission biases that may be challenging for some users to overcome.

To illustrate, the assimilation of altimetry data into ocean models for operational oceanography (e.g., Le Traon et al.,

[1]Ground segment refers to the processing software operated by the space agencies on the ground (as opposed to the onboard software). This software processes raw satellite telemetry into final science products. It includes various components ranging from satellite and data management to technical and science algorithms and a distribution scheme. In the SWOT context, it is also referred to as a science data system (or SDS), as it processes L1B and L2 science products.

2019) requires a continuous set of high-quality and consistent observed products (e.g., Davidson et al., 2019) that must be tackled within a multi-satellite, multi-agency system (e.g., CEOS, 2009; International Altimetry Team, 2021). Various models of the ocean prediction community assimilate Level-3 altimeter products from the multi-mission Data Unification and Altimeter Combination System (DUACS) presented by Dibarboure et al. (2011) and updated by Taburet et al. (2019), Faugère et al. (2022), or Pujol et al. (2023). The system has been operated by CNES and/or Copernicus Marine Service and Copernicus Climate Change Service for almost 3 decades and using 20 satellites. However, all of them were traditional one-dimensional (1D) altimeters.

In that context, the objective of this paper is to give an overview of the 2D Level-3 algorithms and products developed specifically for SWOT/KaRIn as an extension of the operational DUACS system. Section 2 gives an overview of the input data as well as an overview of the L3 algorithm sequence, and Sect. 3 gives more details about each algorithm layer. The Level-3 product and its validation are presented in Sect. 4. Lastly, Sect. 5 discusses and illustrates the relevance and limitations of this dataset for various research domains.

2 Input data and processing overview

2.1 Input data

In this study, we use two types of SWOT Level-2 products. The first one is the geophysical data record of the nadir altimeter instrument (i.e., traditional 1D altimeter), and the second one is the low-resolution (or LR[2]) sea surface height (SSH) product of the KaRIn swath instrument. The "Data availability" section details the data availability and the associated documentation. For both nadir and KaRIn sensors, we use the recommended corrections and reference models from the SWOT project documentation. For KaRIn, we use the sea surface height anomaly (SSHA) variant 2 (model-based corrections), as some corrections from variant 1 are not mature yet. In addition to the product documentation, Raynal et al. (2023), Bohé (2023), and Chen (2023) provide clear practical guidance on the product contents and caveats.

During the calibration process in Sect. 3.3, we combine SWOT data with the along-track Level-3 altimeter products from Copernicus Marine Service/DUACS (see Pujol et al., 2016, or Taburet et al., 2019, for more details). More specifically, we use the following satellites: Jason-3, Sentinel-6/3A/3B, SARAL, CRYOSAT-2, and HaiYang-2B.

Furthermore, to get a background view of the conventional altimetry 2D ocean topography in some figures, we also use the gridded Level-4 maps from the same DUACS system: Ballarotta et al. (2019) have reported that they provide an accurate view of medium-to-large ocean mesoscale systems. Lastly, in some sections, we make some comparisons between KaRIn and maps of chlorophyll concentrations or sea surface temperatures from Copernicus Marine Service (see details in the "Data availability" section).

[2]LR is also used to describe the low-rate-telemetry output of the KaRIn instrument. The resolution and posting are 500 and 250 m, respectively. KaRIn also produces high-rate (HR) data for inland areas and hydrology, with a resolution of 15 to 60 m.

2.2 Overview of the L3 processing sequence

In this study, we used an extended 2D version of the Level-3 algorithm sequence presented by Dibarboure et al. (2011) and updated by Taburet et al. (2019) or Pujol et al. (2023) among others: more details are also provided by the Copernicus Marine Service operational documentation (see the "Data availability" section).

An overview of the SWOT algorithm sequence is presented in Fig. 2: it has two separate components. The first part is the left-hand side (blue items), where we input the 1D nadir altimeter product from SWOT in addition to all other nadir altimeters into the classical DUACS/L3 sequence. In this sequence, SWOT Level-2 products are harmonized with other satellites (e.g., geophysical corrections, models, mean sea surface) in order to get consistent and state-of-the-art datasets for all sensors. More specifically, we use the DT-2024 standards defined by Copernicus Marine Service, EUMETSAT, and CNES in the ongoing reprocessing of more than 30 years of altimetry data (see Kocha et al., 2023, and Appendix A). Then the rest of the nadir Level-3 algorithms (Dibarboure et al., 2011; Taburet et al., 2019) are used in the following sequence: detection of spurious measurements (also known as the editing step), calibration to the reference altimeter (here, Sentinel-6), and reduction in the long-wavelength errors (or LWE) to mitigate residual biases between all sensors. At the end of the nadir sequence, the 1D SWOT nadir altimeter is integrated and is consistent with other altimetry satellites.

All the Level-3 nadir products are then used as inputs for the second part of the SWOT processing, where we integrate KaRIn 2D images into the multi-mission framework (Fig. 2, yellow items on the right-hand side). As for the nadir altimeter, we align KaRIn's geophysical corrections with the DT-2024 standards (detailed in Sect. 3.1), then we edit out spurious or very suspicious pixels (specific 2D editing detailed in Sect. 3.2). The data-driven calibration is then activated to mitigate KaRIn systematic errors and to make the 2D images more consistent with other sensors (detailed in Sect. 3.3). Then KaRIn images go through a noise-mitigation algorithm (detailed in Sect. 3.4) before SSHA derivatives such as geostrophic velocities and vorticity can be computed (detailed in Sect. 3.5). Finally, the Level-3 products from the KaRIn and nadir altimeters of SWOT are blended into a single product, where the nadir altimeter is the center column between the two ribbon-shaped 2D images of KaRIn.

A step-by-step view of the processing sequence is shown for an arbitrary region in the Gulf Stream (Fig. 3). In panel

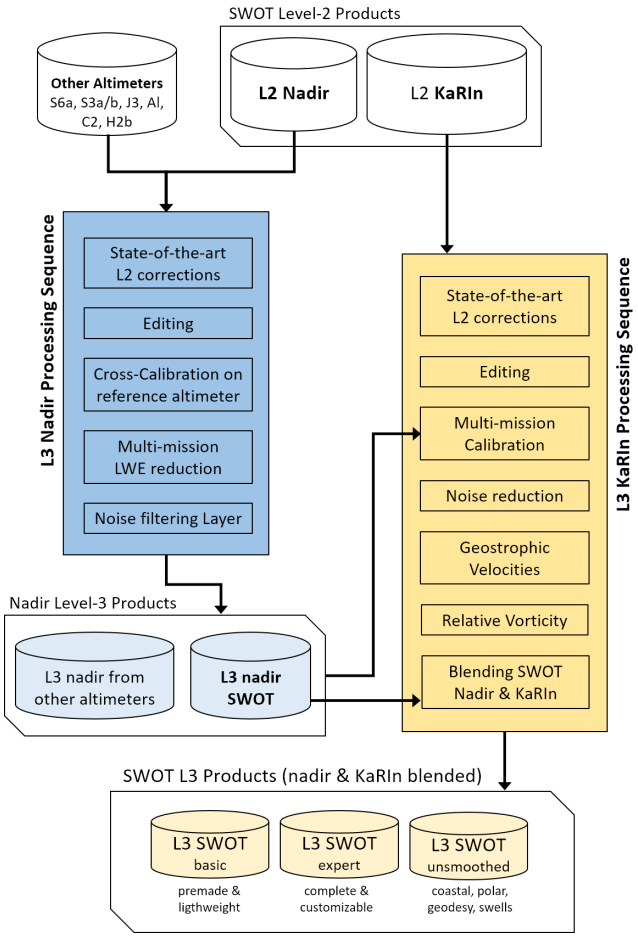

Figure 2. Overview of the Level-3 algorithm and datasets.

(a), the uncalibrated SSHA input from the Level-2 product is used. In this example, SWOT's systematic errors can be as large as tens of centimeters, i.e., hiding the SSHA signal of interest. In panel (b), the Level-3 calibration has been applied, and the systematic errors (e.g., image tilt from spacecraft roll) are mitigated: the actual SSHA emerges with clear mesoscale eddy signatures and good consistency between the ascending and descending images. However, various artifacts remain in the image (e.g., blue spots near 32.5° N). These specific artifacts are caused by heavy rain cells that impact the Ka-band signal. Panel (c) shows the SSHA once the Level-3 editing process has been applied to take out spurious or suspicious pixels. Panel (d) is when we applied the noise-mitigation algorithm: in this panel, the difference might seem small, but Sect. 3.4 will illustrate that even KaRIn's millimeter-scale noise is amplified in the spatial derivatives. The noise-reduction algorithm makes it possible to use the SSHA to observe very small ocean features (e.g., internal waves; see Sect. 4.1) or to calculate derivatives such as geostrophic velocity and vorticity (Fig. 3e and f).

2.3 Output data

The Level-3 products generated by this sequence have three variants, aligned with the Level-2 nomenclature. The "basic" variant is the most lightweight and simple to use, as it contains only a pre-made SSHA at 2 km resolution that is directly usable by oceanographers. In contrast, the "expert" variant contains each individual Level-3 layer (each processing step from the KaRIn block in Fig. 2). The general objective for the expert product is to have a sandbox product so that the SWOT and altimetry communities can investigate the different processing steps in more detail. More specifically, the rationale is threefold:

- Firstly, the Level-3 algorithm is a research-grade product that aggregates state-of-the-art algorithms and corrections from various groups. These components may need to be evaluated separately by an expert community. This can be done with the expert variant, as the Level-2 and Level-3 products can be combined to evaluate only some components of the L3 product. To illustrate, some processing steps such as the calibration might be deemed unnecessary or even detrimental by some users, and the expert variants make it possible to customize the L3 content to each domain.

- Secondly, various research groups may be able to develop better alternatives to some Level-3 layers, and the expert product gives a simple medium for them to test their algorithm and to evaluate the strengths and weakness independently from other Level-3 layers. In other words, the expert L3 product is a simple test bed to evaluate future algorithms and corrections.

- Thirdly, the expert product can contain duplicate/alternative layers with experimental algorithms that are operated globally for large-scale evaluations. To illustrate, the basic variant must contain a single default state-of-the-art correction for tides, whereas the expert variant can integrate one or two extra tidal models that are under evaluation by the community. With this pre-made Level-3 variant with multiple models, any Level-3 user will be able to evaluate the strengths and weakness of the experimental tidal models even if they are not a tide expert, let alone able to operate or run the tidal models. The L3 user feedback then makes it possible to consolidate how the L3 standards should evolve in the future.

To summarize, the basic L3 variant is aimed at studies for researchers who do not want to get into the details of SWOT algorithms or mission-specific biases: they can get an off-the-shelf SSHA for thematic studies. In contrast, the expert variant is aimed at altimetry algorithm and correction experts who *do* want to get into the technicalities of SWOT and altimetry standards.

There is also a third variant: the "unsmoothed" Level-3 product, which is derived from the eponymous Level-2 prod-

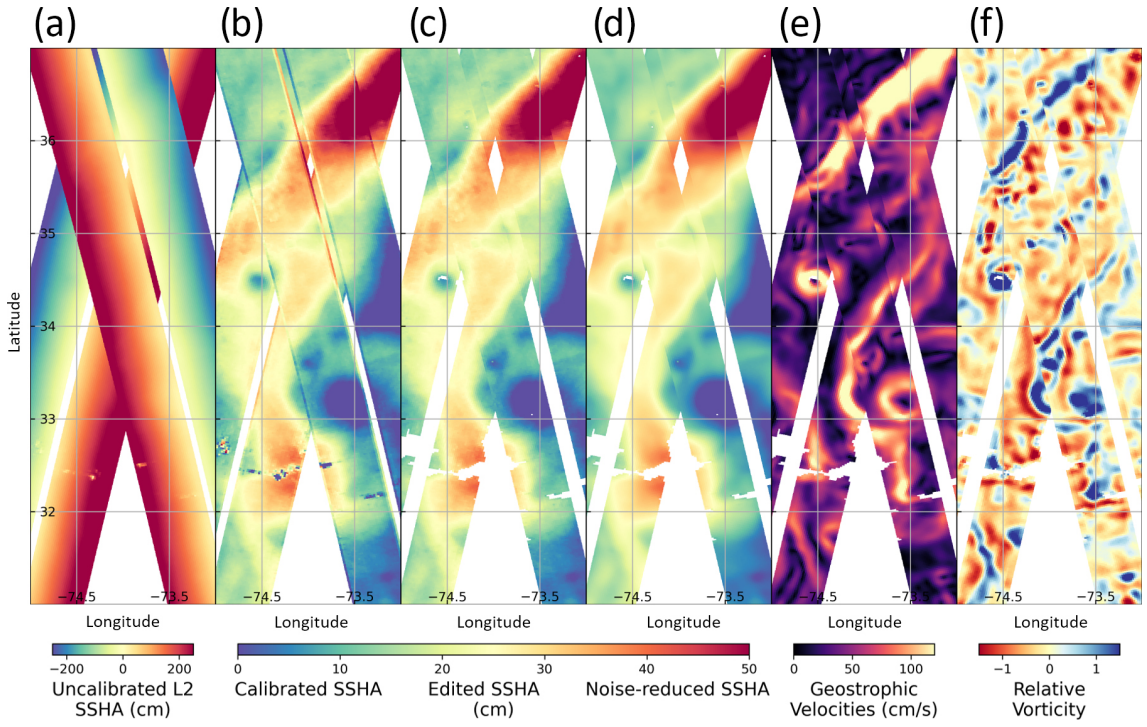

Figure 3. Example of a KaRIn segment (Gulf Stream region) at various steps of the Level-3 processing sequence. Panel **(a)** is a map of the Level-2 SSHA (uncalibrated) at the beginning of the Level-3 sequence. Panel **(b)** is the same scene once the Level-3 data-driven calibration is applied. Panel **(c)** is when the Level-3 editing procedure is applied to get rid of spurious pixels (here heavy rain cells and biased swath edges). Panel **(d)** is when the noise-mitigation algorithm is applied. Panels **(e)** and **(f)** are the SSHA derivatives computed from panel **(d)**.

uct of the ground segment. This variant leverages the 250 m resolution of the KaRIn LR mode, whereas the basic and expert modes are built from the 2 km products. Strictly speaking, this is a third processing block since the input L2 product for KaRIn is different. However, in practice, the algorithm sequence is the same: the only difference is that the input unsmoothed L2 product must be given many missing parameters or geophysical corrections that are not provided by the ground segment at 250 m. The rationale for the unsmoothed Level-3 product is to provide a simple, off-the-shelf 250 m product with all the necessary content for coastal, geodesy, or sea-ice users. To achieve this, we keep only critical content from the 250 m product, we add certain geophysical models that might be needed for future standard upgrades, and then we add our Level-3 layers. Finally, we use a more convenient product structure that is similar to the basic and expert formats, whereas the Level-2 unsmoothed format was designed by the SWOT project for technical and instrument-oriented studies.

2.4 Level-3 product versions

At the time of this writing, the Level-3 product is available in two versions: v0.3 and v1.0. Version 0.3 was made public on the Archiving, Validation, and Interpretation of Satellite Oceanographic Data (AVISO) website in December 2023, and the more up-to-date Level-3 version 1.0 was released in May 2024 (see the "Data availability" section). For the sake of clarity in this paper and because many beta glitches are now fixed, we describe only the v1.0 Level-3 algorithms, although this paper contains some original images from 2023 and v0.3. An overview of the differences between v0.3 and v1.0 is given in Appendix A.

3 Level-3 step-by-step algorithm description

3.1 Updating L2 algorithms

The Level-2 products from SWOT were defined approximately 2 years before launch. They integrated state-of-the-art corrections (e.g., sea-state bias, tidal models) and reference surfaces (e.g., mean sea surface, mean dynamic topography) at the time. But the state of the art has evolved since then. More generally, each satellite has some periodic upgrades to standards that are not coordinated between multiple agencies and programs. The first Level-3 processing step is to align these standards between all missions and to ensure that SWOT products use the latest recommendations from the Ocean Surface Topography science team and SWOT science team: all missions are upgraded consistently at any given time.

To illustrate, at the time of this writing, the Level-2 product version C from SWOT is not aligned with the DT-2024 standards from Kocha et al. (2023)[3], although it will likely be upgraded in the near future. More generally, the details of each upgrade might become obsolete as new corrections and models get integrated and the Level-2 input is adapted to DT-2024, so we will not detail minor upgrades (e.g., ancillary data such as the distance to the coast, the shoreline, and the sea-state-bias implementation). However, there are at least three noteworthy items for the Level-3 product: the barotropic tidal model, the mean dynamic topography, and the mean sea surface.

The DT-2024 standards selected the latest iteration of the FES22 (finite-element solution) barotropic tidal model (Lyard et al., 2025; Carrère et al., 2023) after a side-by-side comparison with other recent tidal models. FES22 significantly reduces the measurement errors in many coastal regions (Fig. 4). The improvement measured with Jason-3 can be as large as 2 to 4 cm^2 for the coastal ocean, whereas the TOPEX/Jason ground track was assumed to be well-charted for tides. Similarly, for higher latitudes not covered by Jason-3 and particularly for the Arctic Ocean, the FES22 model was reported by Carrère et al. (2023) to reduce the variance by 2 to 5 cm^2 in the deep ocean and 20 cm^2 or more in coastal regions. Beyond the specific case of FES22, the barotropic and baroclinic tidal models are extremely important for SWOT because it is the first mission able to chart all coastal regions with 2D images at 250 m or 2 km resolution and with high precision. Therefore, the SWOT 2D images are much more affected by tidal model residual errors since they are observing new geographical zones compared to the 1D repeat ground tracks such as the TOPEX to Sentinel-6, ERS to SARAL, or Sentinel-3 satellites. In that context, it is essential for the Level-3 product to stay very close to the published state of the art and to serve as an evaluation sandbox for any new tidal models.

Similarly, the DT-2024 standards use the CLS22 mean dynamic topography (MDT) model from Jousset et al. (2023). This model brings a significant improvement on the 2018 iteration, in particular over the Arctic Ocean. In addition to more complete coverage, the 2022 MDT model also fixes documented artifacts and improves the consistency of independent drifters by 10 % on average and locally often more.

The most essential upgrade for KaRIn is the mean sea surface (MSS) model. At the time of this writing, the Level-2 SWOT product version C is based on the 2015 CNES/CLS model. In contrast, the Level-3 product uses the hybrid 2023 model that blends the best of CNES/CLS22, DTU21, and Scripps22 (see Laloue et al., 2025, or Schaeffer et al., 2023, for details). This model was shown to be significantly better than any alternative, especially for the smaller scales of interest with SWOT. Indeed, the SSHA from KaRIn sometimes exhibits some very unusual features for SSH anomalies (e.g., Fig. 5a from 20 to 22° N, north of the Dominican Republic). The SSHA artifacts are strongly correlated with the bathymetry (Fig. 5b): the strange topography features actually originate from unresolved geoid signatures that the 2015 CNES/CLS MSS model does not correctly represent. This arbitrary example is representative of the many residual geoid signatures that one might see in KaRIn images wherever the bathymetry is rugged, such as over uncharted seamounts, rifts or mid-ocean ridges, and the continental shelf.

Using a better MSS model yields smaller error variance (or power spectral density) in the KaRIn SSHA: this improvement is very clear between the MSS15 model and the MSS23H model (Fig. 5c, derived from Laloue et al., 2025). While the MSS has essentially no impact on scales below 10 km or above 70 km, there is a critical range of wavelengths from 10 to 70 km where the old MSS model from 2015 increases the variance by as much as 90 %. Moreover, it tends to distort the power spectral density (PSD) shape by adding a hump-shaped artifact: this artifact is fully explained by the MSS error (red and blue lines). These observations are not surprising, as they were predicted by Pujol et al. (2018). The new hybrid MSS model is also beneficial for traditional 1D altimeters but not as much: their measurements are increasingly contaminated by instrument noise below 70 km, so the MSS errors are less impactful than those for KaRIn. To illustrate, the thin black and gray lines from the two MSS models applied to the SWOT nadir altimeter differ by only 10 % from 10 to 70 km. In contrast, having an accurate MSS model becomes crucial for the KaRIn SSHA because of the very high precision of this instrument.

Despite the improvement brought by the 2023 MSS model, there are still many regions where residual geoid features are very noticeable, as in Fig. 5a. Therefore, it remains extremely important to keep improving MSS models for the critical scales ranging from 10 to 70 km. In that context, by far the main asset for the long term is the KaRIn SSH measurement itself, as it can be averaged into a local mean sea surface or mean profile (Dibarboure and Pujol, 2021; Yu et al., 2024).

3.2 Editing spurious pixels

The Level-2 product contains a large number of quality flags, which provide a flexible way to remove spurious pixels. In addition to the Level-2 product documentation ("Data availability" section), Chen (2023) explain their meaning in detail, and they provide general guidelines of how to use them. While extremely useful, these flags are sometimes based on theoretical uncertainty, and they do not always capture the reality of suspicious/spurious pixels. Some flags, such as the sea-ice flag, radiometer rain flag, or KaRIn wave quality flags (among others), are sometimes detrimental: they tend to remove large segments of good data. In contrast, none of the Level-2 flags properly capture obvious anomalies such as heavy rain cells or some sea ice. Moreover, the shore-

[3]The details of the DT-2024 standards are given in Appendix A

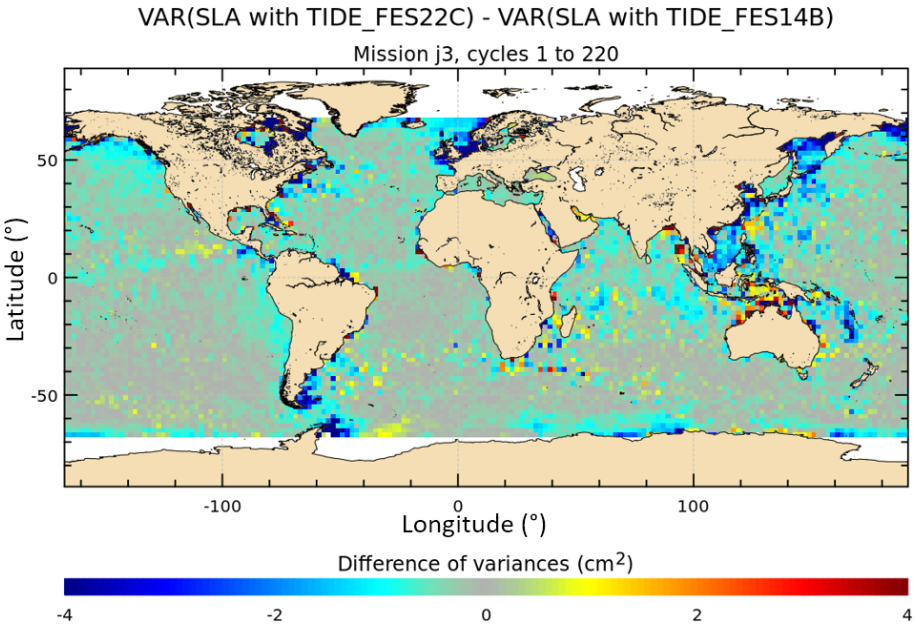

Figure 4. The SSHA variance difference (FES22 correction vs. FES14B correction). Negative values indicate that the new FES model provides a better correction of the residual tidal signal.

line mask used to discriminate between land and sea in the ground segment is not always reliable, resulting in uneven flagging of the shorelines and islands, with detrimental effects in coastal zones.

In order to improve the spurious pixel and outlier detection, the Level-3 processing uses a more practical and data-driven editing sequence. More precisely, the L3 editing uses the following incremental steps of decreasing importance:

- Flag value 102 suppresses defaulted SSHA values (e.g., because of missing KaRIn SSH or geophysical corrections and models).

- Flag value 101 suppresses pixels over land using a shoreline mask. This step is similar to the land flag in the Level-2 product but is based on a custom land/sea/island/lake mask combining different sources (e.g., Open Street Map or Global Island).

- Flag value 100 suppresses pixels if the KaRIn Level-2 quality bit $2^8 = 256$ is raised but only for the edges of each swath. The edges are at the limits of the KaRIn coverage, and they are not always properly covered at 250 m, resulting in various artifacts when the data are averaged down to 2 km. Although these columns are beyond the SWOT requirements (10 to 60 km), we do try to keep the edges when their coverage is good enough.

- Flag value 70 suppresses pixels impacted by spacecraft events (e.g., gyrometer calibration, maneuvers, eclipse transitions[4]) based on the Level-2 quality bit $2^{11} = 2048$. Most of these events can affect the SSHA quality.

- Flag value 50 suppresses abnormally high SSHA values in coastal and polar regions, as they are generally caused by land or ice contamination in mixed pixels (i.e., an iceberg in an ocean pixel or a layover from land or sea ice).

- Flag value 30 suppresses SSHA pixels that are out of the expected statistical distribution, i.e., a custom lookup table based on the KaRIn noise as a function of significant wave height.

- Flag value 20 suppresses the KaRIn-based L2 quality bits $2^8 = 256$ and $2^{30} = 1\,073\,741\,824$ in polar regions. This step removes suspected sea-ice pixels. Note that this editing layer tends to be very conservative and to keep only open ocean pixels: users who want to study the polar ocean in the presence of sea ice may want to ignore this editing layer in order to keep as much coverage as possible.

[4]Most of the orbital circle of the satellite is illuminated by the Sun, but a smaller fraction is in the shadow of the Earth (the eclipse segment). When the satellite transitions from illumination to eclipse (or the opposite), there is a substantial and rapid change in thermal conditions for the instrument and the platform. So the eclipse transitions are excluded from science requirements because the satellite is not in a stable and nominal condition. In the current product release (Level 2, version C), the SWOT project flags about 2 min of data after each transition as a buffer for the satellite to stabilize.

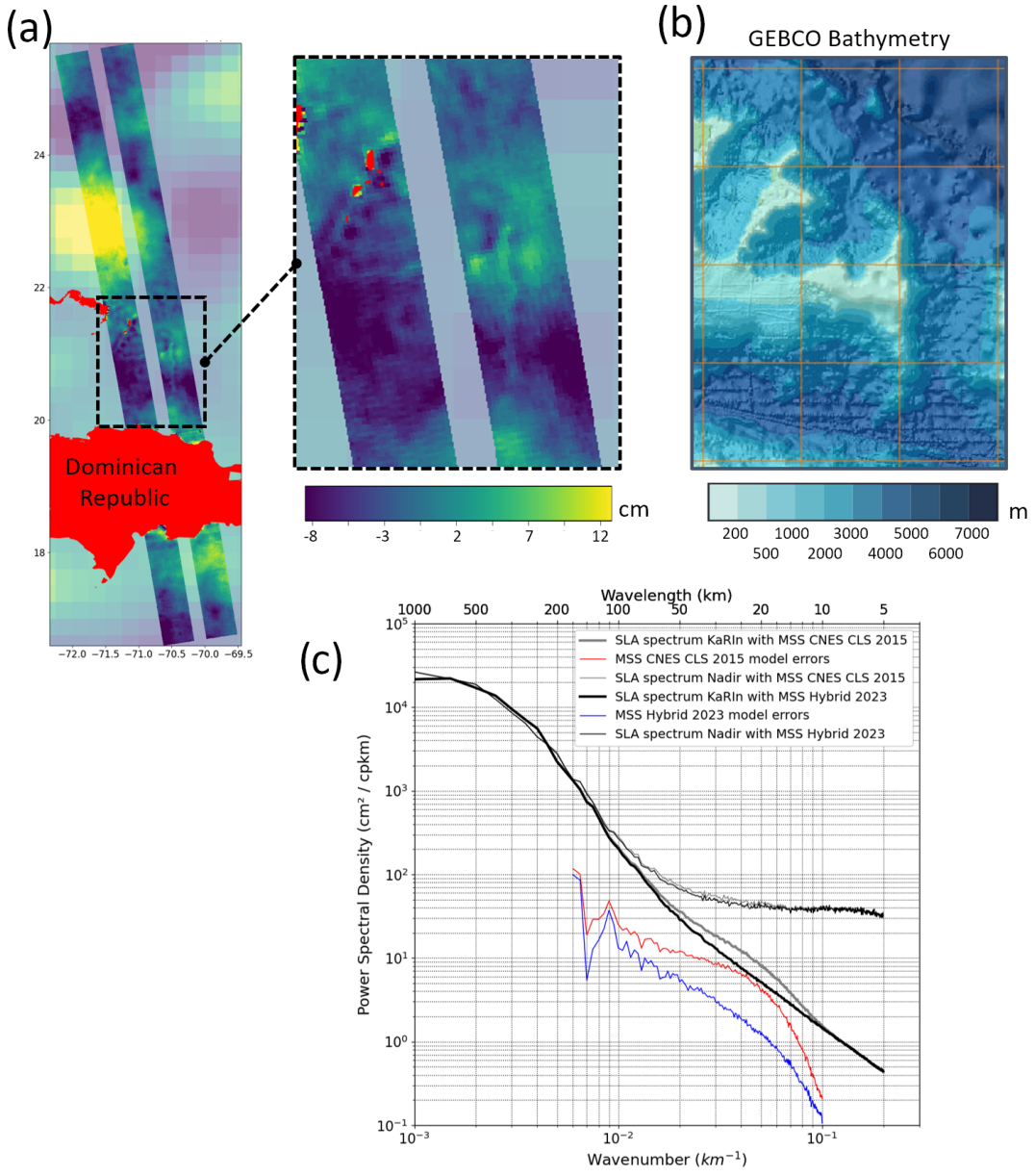

Figure 5. Importance and limitations of current mean sea surface models for SWOT. Panel **(a)** shows a SWOT/KaRIn SSHA segment in the Caribbean Sea and tropical Atlantic Ocean (SWOT 1 d phase), with a zoom north of the Dominican Republic. Panel **(b)** shows the GEBCO bathymetry in the same region. Panel **(c)** shows the power spectral density of the KaRIn (thick solid line) and nadir SSHAs (thin solid line) when they are based on the CNES/CLS2015 mean sea surface model (gray) and when the CLS/Scripps/DTU hybrid 2023 model is used instead (black). The red/blue lines are the estimated errors in each MSS model.

– Flag value 10 suppresses all pixels flagged in the Level-2 product if they are less than 5 km from the coast and are flagged in the Level-2 product (parameter ssha_karin_2_qual $>2^8$). In the last couple of coastal pixels, various anomalies may appear from KaRIn measurements or from geophysical corrections (e.g., imperfect tides or atmospheric correction, imperfect mean sea surface models). Therefore, this editing layer tends to be conservative to keep only trustworthy pixels based on Level-2 flags: users who want to keep as much coastal coverage as possible may want to ignore this editing layer.

– Flag value 5 suppresses all pixels that deviate from a locally smoothed version of the KaRIn SSHA (Gaussian filter, cutoff of 20 km). The purpose of this step is to identify smaller-scale discrepancies such as ships, icebergs, or tiny isolated rain cells that were not detected by the previous steps. This last layer is not ap-

plied in a handful of regions with very large internal tide signatures (north of Brazil; Madagascar, Indonesia and Malaysia; and the Bay of Bengal). For these regions, it tends to be too conservative and to misinterpret the sharpest internal wave crests or troughs as spurious regions. We think it is better to leave some rain cells rather than altering actual content in a systematic way, at least until a better editing layer can be developed.

To summarize, our L3 editing flag falls into one of four categories:

- 0 means that the pixel went through all the editing layers and is considered good;
- 10 or less means that the pixel is suspect, so it is recommended to ignore it if the user wants to make sure they keep only the best quality;
- 11 to 99 is a mixed bag of bad indicators of increasing importance, and it is recommended to ignore these pixels unless more coverage is really needed (e.g., coastal regions; see below);
- 100 or more means that it is strongly recommended not to use the pixel, as it is very likely unusable or defaulted.

Three examples of SSHAs are given in Fig. 6: before editing (left column), after editing (center column), and the corresponding editing flags (right column).

- Panel (a) is a typical example of flag values of 100 or more (red regions), where we discard cross-track distances beyond the nominal 10 to 60 km. It is also an example of a flag value of 70 in an eclipse segment: in this particular example, the SSHA data are fine, even if the L2 product has raised the mission event flag (discussed below). Lastly, the spurious pixels from rain cells are captured by lower flag values (typically flag values of 20 to 70, i.e., cyan pixels in the right panel).
- Panel (b) is an example of a coastal region where intermediate flag values tend to remove the last coastal pixels, while higher values remove the land pixels. In this particular region, the coastal SSHA is likely degraded by geophysical corrections rather the KaRIn measurement itself. So, removing these pixels is a questionable and subjective choice. For many users, taking out degraded SSHAs makes sense. However, the only way for some experts to retrieve better MSS or tidal models with SWOT data is to keep these pixels as inputs to their studies. Consequently, tides and MSS communities may prefer to ignore some of these quality flags.
- Panel (c) is an example of a region with massive internal tides: the challenge here is to isolate rain cells while not removing the smaller scales of internal tides. In this particular example, the editing is working well, but in other regions, it might be too aggressive and remove useful internal tides or internal waves. To summarize, the current L3 editing layers do a good job of removing spurious pixels that are not always captured by Level-2 flags, but they may be over-aggressive in ambiguous situations.

Moreover, the editing mechanism behaves differently at 2 km (Fig. 7a and c) and 250 m (Fig. 7b and d):

- The first example is in the southern Pacific Ocean, with a mix of mesoscale and internal waves and some rain cells, with some (expected) spurious pixels for the columns on the swath edges[5]. In this particular scene, the 2 km editing takes out the swath edges (red and orange pixels on the right-hand-side editing flag map). Then the bulk of the rain cell is isolated by intermediate editing layers (green pixels on the editing flag map). Finally, the last layers capture leftover pixels and rain cell boundaries (blue pixels on the editing flag map). The full editing flag tends to clean up most of this scene, but it is also somewhat aggressive, as it destroyed a fraction of the internal wave feature. In contrast, the 250 m editing algorithm leverages the full resolution to isolate smaller clusters of spurious pixels, some of which would be averaged down to 2 km, and causes a small but significant degradation of the 2 km pixel that is not captured by the 2 km editing.
- The second example is in a sea-ice-covered region of the Southern Ocean. As expected, the 2 km resolution provides coarse topography measurements, where it is complex if not impossible to properly identify spurious pixels. Conversely, the 250 m editing retrieves more consistent coverage, with sharper detection of lead-to-floe transitions or ice/ice transitions. While this current editing algorithm was not designed to classify the surface type, this specific example illustrates the capabilities of the 250 m resolution and the potential to finely separate the ocean from the sea ice in the future.

Quantitatively, on average, 15 % of the KaRIn pixels are edited out if we include flag values of 70 and 100. This value is also expected: the main contributor is the Level-2 quality bit 256, which is very often raised for cross-track distances beyond the 10 to 60 km requirements (i.e., approximately 8 % of the time). Therefore, the KaRIn Level-3 algorithms flag approximately 7 % of invalid pixels in the nominal 10–60 km swath. That number includes the data flagged during the eclipse transitions (3 % to 4 %).

[5]Most of these artifacts have two causes: the phase screen correction, which is not final in the L2 version C, or the 250 to 2 km averaging process in a fixed geographical grid. The former exists at both resolutions, while the latter exists only in the 2 km resolution products but not in the native 250 m pixels.

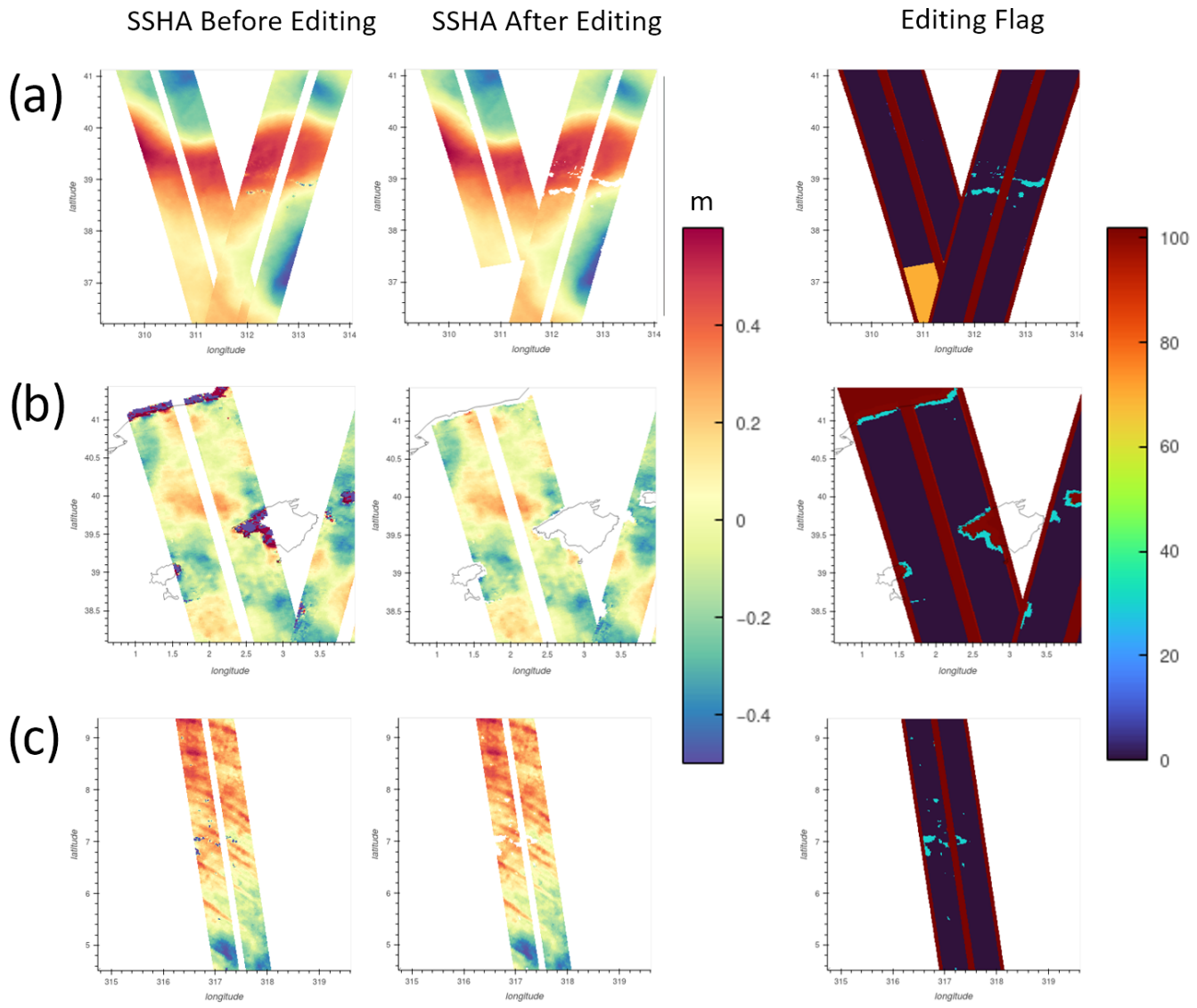

Figure 6. Examples of SSHA editing. The left panels are raw SSHA measurements before the editing process. The center panels are the SSHAs after the L3 editing process. The right-hand-side panels are the editing flag values. Panel **(a)** is an example of a rain cell, located in the Gulf Stream (cycle 538, passes 7 and 20). Panel **(b)** is an example of a coastal region, located in the Mediterranean Sea (cycle 538, passes 3 and 16). Panel **(c)** is an example of internal waves, located off the coast of Brazil (cycle 538, pass 20).

During the eclipse transitions, KaRIn is no longer constrained by its requirements, as conservative prelaunch predictions assumed that the instrument would need a couple of minutes to stabilize to the new thermal conditions. However, recent analyses find that the data have a nominal quality during the eclipse transitions and that they should probably not be flagged. Unfortunately, eclipse transitions are currently flagged in the Level-2 product in an irreversible way: a single L2 quality bit is used to flag all mission events. In the current L3 release, we do not isolate the eclipse transitions from other events. Future releases of the L2 or L3 products will probably retrieve the 3 %–4 % of data that are currently edited out incorrectly during these eclipse events.

If we ignore the swath edges and eclipse transitions, which are excluded from the mission requirements, we have approximately the same fraction of edited pixels as nadir altimeters (3 % to 4 %). Moreover, this percentage increases in specific regions (Fig. 8a): e.g., polar regions (expected from sea ice); in rain regions, as for SARAL and its Ka-band nadir altimeter (e.g., Picard et al., 2021); and in some coastal regions. For the latter, the fraction can be very large in some places (up to 50 % for the last couple of coastal pixels): we suspect that geophysical corrections and incorrect MSS models are the primary sources of error, at least up to the last pixel where KaRIn SSH artifacts start to dominate.

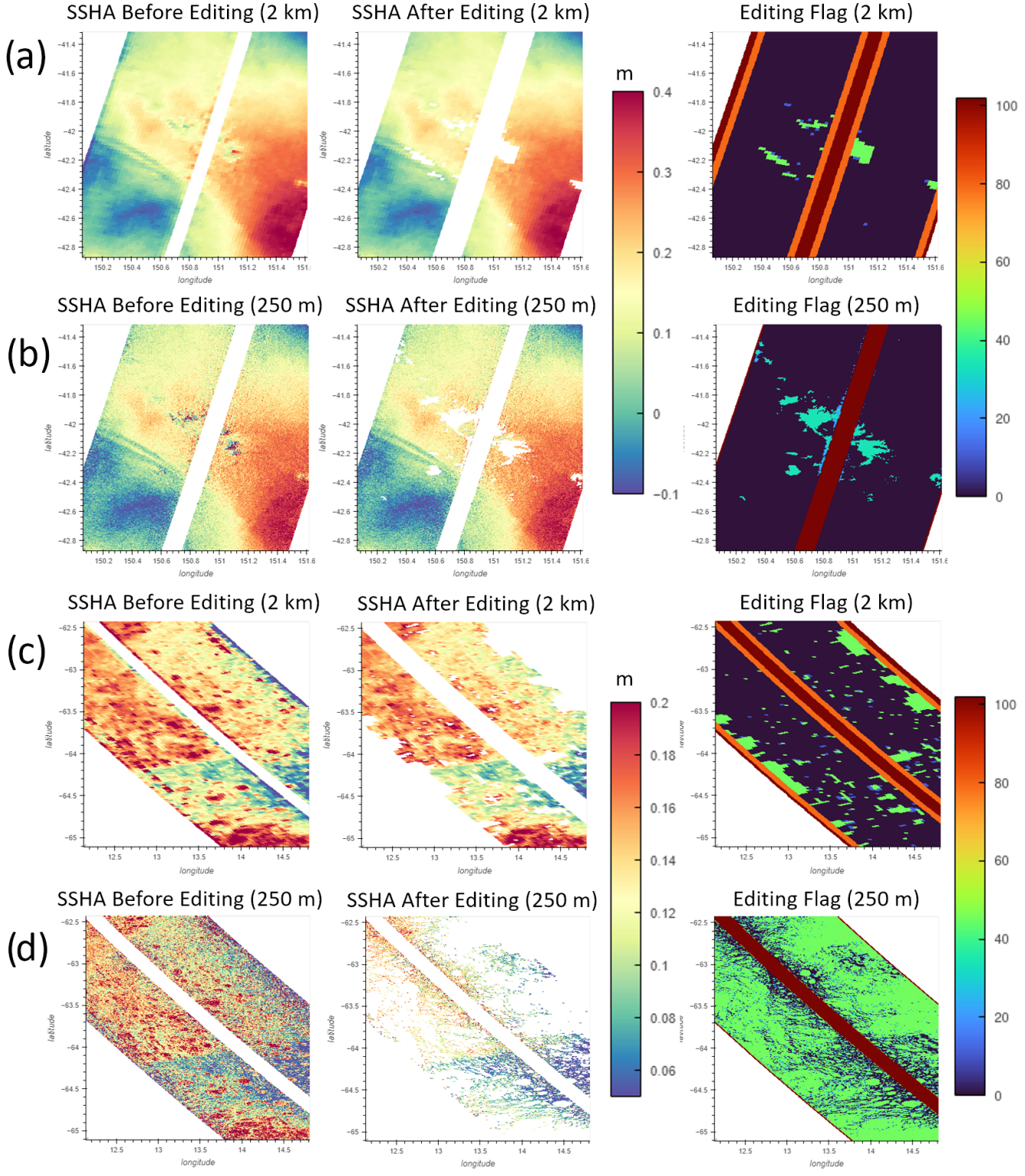

Figure 7. Examples of two editing scenes at 2 km (panels **a** and **c**) and their 250 m counterpart (panels **b** and **d**). Panels **(a)** and **(b)** are in the southern Pacific Ocean. Panels **(c)** and **(d)** are in a sea-ice-covered region of the Southern Ocean. The left panels are the raw SSHAs before the editing process. The center panels are the same after the L3 editing process. The right-hand-side panels are the editing flag values.

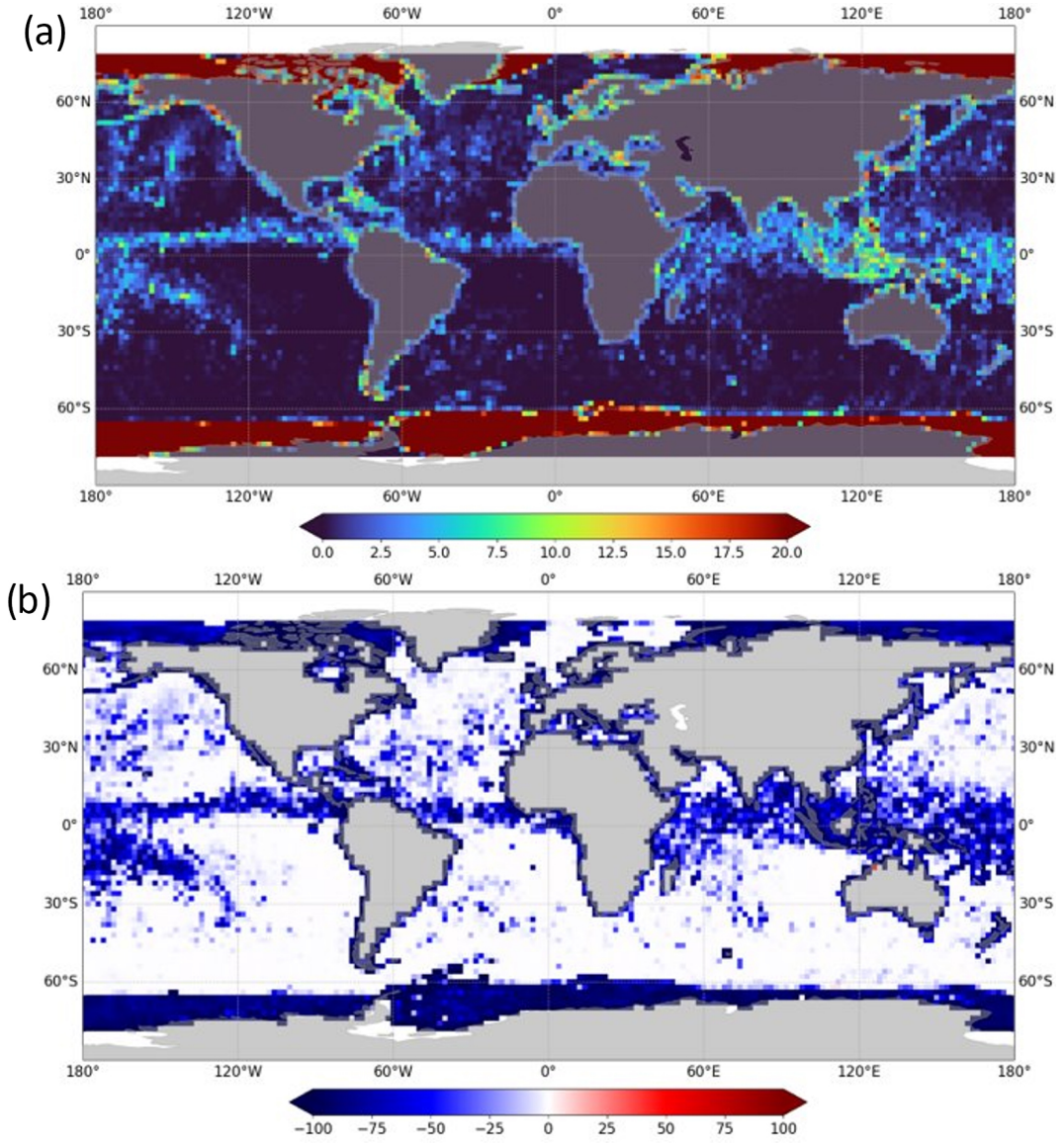

Figure 8. Impact of the Level-3 editing layer on the SSHA. Panel **(a)** shows the percentage of data edited out in the Level-3 product from the 10 to 60 km cross-track. Panel **(b)** shows the variance reduction (in cm^2) when spurious data are edited out. Note that in both panels, we ignore SWOT's eclipse transition segments.

Still, the editing layers do meet their primary objective: the SSHA variance is reduced when the editing flag is applied vs. when it is not (Fig. 8b). The dark-blue region where the variance is reduced after editing is very consistent with the tropical rain regions observed by SARAL (Picard et al., 2021) with or sea-ice regions. In these regions, the L3 editing reduces the variance by up to 50 cm^2: this highlights that it is essential to take out spurious pixels from KaRIn images, as they might induce artifacts that are large enough to affect oceanography studies. However, the L3 editing also removes a large amount of variance in some coastal regions, which might be more questionable. Without a solid ground truth or trustworthy validation metrics, we cannot determine if it is correctly removing artifacts from tides and MSS models or if the editing also removes actual ocean features of interest as well.

Therefore, the editing layer is optional in the Level-3 product, so any expert user can decide to use it or not or even design their own editing strategy. In the basic variant of the Level-3 product, all editing layers are applied by default, whereas the expert variant has the flag itself and the unedited SSHA: the L3 user can therefore opt to keep only some editing layers if they want. This is particularly useful for lower values of the editing flag, as these layers can be somewhat subjective, and we have no ground truth to parameterize them with confidence. To illustrate, polar and coastal users may

prefer to suppress only the pixels with an editing flag of 70 or more. They will get more coverage but also more suspicious pixels: this strategy would also make sense for MSS or tide experts who want to get as much coverage as possible since they have their own theme-specific algorithms to suppress residual outliers.

3.3 Data-driven calibration

The images provided by KaRIn can be biased or skewed by a few centimeters to tens of centimeters (e.g., Fig. 3a). There are various sources of errors: e.g., uncorrected satellite roll angle, interferometric-phase biases, thermoelastic distortions in the instrument baseline, and antennas. In order to mitigate these topography distortions, it is necessary to use a calibration mechanism based on the interferometric phase or topography data, hence the name data-driven calibration. Dibarboure et al. (2022) give an overview of the calibration of KaRIn images: why a calibration is needed, how it can be performed, and what the expected performance before SWOT's launch was. Moreover, Ubelmann et al. (2024) provide a post-launch update, giving the magnitude of the systematic errors observed in real data and the residual error once data-driven calibration is applied. While the technical details are beyond the scope of this paper, this section intends to give a quick summary of the items of interest for the Level-3 expert users; standard ocean users can probably skip it and move on to Sect. 3.4 (noise mitigation).

In both calibration papers, two variants of the calibration are described: the SWOT single mission, or Level-2 algorithm, and the multi-mission, or Level-3 algorithm. As the names imply, the former is used in the SWOT ground segment and L2 products, whereas the latter is specific to Level-3 processors. The L2 algorithm was primarily designed to meet the hydrology error budget (SWOT, 2024) that is dominated by the larger scales (typically 7000 km or more) of the systematic errors. This L2 algorithm is considered optional over the ocean: SWOT ocean requirements are defined only from 15 to 1000 km, where no data-driven calibration is needed. Although optional, the L2 calibration remains beneficial over the ocean as well because it is able to reduce large-scale ocean errors even if they are formally beyond the scope of the mission objectives. The L2 algorithm is based on SWOT data only because a ground segment cannot depend on external satellites.

In contrast, the Level-3 algorithm was designed to leverage better algorithms and external satellites: not only Sentinel-6, the climate reference altimeter, but also all other altimeters in operation (Sentinel-3A/3B, HY2B/C, SARAL, Jason-3, CRYOSAT-2). The L3 correction is generally more robust and stable than the Level-2 variant thanks to the thousands of daily multi-mission crossover segments provided by the constellation.

$$\mathrm{SSHA_{cal}}(t,b) = \mathrm{SSHA_{uncal}}(t,b) + \mathrm{XCAL_{L3}}(t,b), \tag{1}$$

where $\mathrm{XCAL_{L3}}(t,b) = B_{\mathrm{L3}}(t) + b \cdot L(t) + b^2 \cdot Q(t) + \mathrm{PS_{L3}}(b,t) + \mathrm{SC}(b)$ (2)

and $B_{\mathrm{L3}}(t) = B_{\mathrm{KaRIn|nadir}}(t) + B_{\mathrm{nadir|S6}}(t) + B_{\mathrm{nadir|lwe}}(t)$. (3)

From a practical point of view (Eq. 1), the basic variant of the Level-3 product contains a calibrated topography ($\mathrm{SSHA_{cal}}$), whereas the expert variant provides both the original/uncalibrated topography ($\mathrm{SSHA_{uncal}}$) and the correction ($\mathrm{XCAL_{L3}}$). The rationale is to give some flexibility to the users who want to use their own calibration instead. The calibration is provided per pixel, i.e., in 2D as a function of time t (the along-track coordinate) and cross-track distance b (the cross-track coordinate). The correction has five components (Eq. 2):

- B_{L3} is a time-evolving bias per swath.
- L is a time-evolving linear cross-track correction per swath.
- Q is a time-evolving quadratic cross-track correction per swath.
- $\mathrm{PS_{L3}}$ is our empirical estimate of the phase screen: a small and slowly time-evolving bias that changes in the cross-track direction; see Peral et al. (2024) for more details.
- SC is the static calibration of the $B/L/Q$ parameters (mean value throughout the mission's lifetime).

At the time of this writing, the bulk of the SC parameter is already accounted for in the Level-2 algorithms (e.g., meter-scale tilt of each image from the mean L, decimeter-scale curvature from the mean Q parameter). The residual SC component that we retrieve in the L3 product is probably explained by the period when the mean was computed: the static calibration of the ground segment was computed in spring 2023, while our residual SC was recomputed over a much longer time series and a consistent set of beta angles. As for the phase screen $\mathrm{PS_{L3}}$, we retrieve an error on the order of ± 4 mm: most of the error is time invariant, although a fraction of ± 1 mm continuously evolves along the orbit circle (the error changes with latitude, and it is different for ascending and descending passes). Note that in the future, it is likely that the PS (phase screen) and SC (static calibration) components will be zero, as they should be corrected in the reprocessed Level-1B algorithms.

Conversely, the primary purpose of the data-driven calibration is to handle the time-evolving errors $B/L/Q$, i.e., a second-order polynomial function of b for each swath for each time step t. Ubelmann et al. (2024) confirm with flight data that the prelaunch strategy from Dibarboure et al. (2022) is relevant. Before the data-driven calibration, they observe various scales in the $B/L/Q$ errors: very slow drifts of the order of a few months, cyclic beta-angle variations of a few

weeks, more rapid changes on the order of a few days, harmonics of the orbital revolution period, and random higher frequencies (e.g., noise from the gyrometer). The order of magnitude of each scale is consistent with prelaunch simulations.

Once calibrated, the $B/L/Q$ errors are strongly reduced. This is typically visible in metrics such as the variance in the measured KaRIn SSHA as a function of the cross-track distance b (Fig. 9a). This variance is the sum of three items: (1) KaRIn's systematic errors (the L and Q terms increase as a function of b), (2) natural SSHA variability from the ocean (on average, it is the same for all cross-track distances), and (3) other KaRIn errors (which are cross-track invariant). Before calibration (not shown), the variance increases away from the nadir position, and it can be as large as 35 cm^2 in the far range and regionally much more. After the Level-2 calibration (green curve), the error is strongly reduced, but the cross-track dependence is still visible for a couple of square centimeters for the 21 d orbit (plain green) and much more for the 1 d orbit (dashed green)[6]. In contrast, after the Level-3 calibration (blue curve), the cross-track dependence is almost removed, and there is no difference between the left and right swaths. In other words, the L3 calibration has strongly reduced the systematic error terms L and Q. The geographical distribution of the standard deviation of the KaRIn SSHA (combining multiple 21 d cycles) does not exhibit any obvious regional anomaly (Fig. 9b): it is very homogeneous and is consistent with its nadir altimetry counterpart (not shown), and the variance is explained by the actual ocean variability.

In order to quantify the residual error and its spectral breakdown, we used a variant of the Ubelmann et al. (2018) methodology. Using cross-spectra between parallel columns of the KaRIn images, we can form a 3D cube of cross-spectra, and we can use 2D frequency slices to separate the signature from correlated errors in the nadir and KaRIn datasets and specifically isolate the systematic error terms $B/L/Q$. The result is shown as a power spectral density (PSD) in Fig. 9c. The black line is the KaRIn SSHA power spectrum (before calibration), and the brown/orange lines are the systematic errors. Before calibration (dark brown curve), the error is mainly described as a K^{-2} power law from 15 to 40 000 km (orbital revolution), and then becomes a flat value for longer time series (multiple revolutions, hourly-to-daily drifts). On top of this background line, there is a series of peaks located on the harmonics of the orbital revolution periods (thermoelastic distortions). In practice, this error PSD is very similar to the prelaunch simulated errors from Dibarboure et al. (2022): no significant changes to the calibration algorithms were necessary with actual flight data.

As expected from prelaunch simulations, both calibrations reduce the systematic error for longer wavelengths, by a factor of 10 for the L2 product (Fig. 9c, orange curve) and by a factor of 50 for the L3 product (Fig. 9c, light brown). The L2 calibration starts to be significantly effective near 5000 km, whereas the L3 one starts near 1000 km. For scales smaller than 1000 km, KaRIn meets its requirements (red line, from 5 to 1000 km) without any form of calibration. Integrating the PSD for all wavelengths, the error after L2 calibration is on the order of 2.5 cm, and after the L3 calibration, the residual error decreases to 1.5 cm rms. Most of the variance is located at the larger scales and probably originates in leakage of the ocean variability (e.g., uncorrected biases and slopes from barotropic corrections that might be confused with KaRIn errors).

The calibrated results are consistent with the prelaunch simulations from Dibarboure et al. (2022). This is not surprising because the *uncalibrated* errors are also consistent with prelaunch simulations, and the algorithms are unchanged. Ubelmann et al. (2024) make a more in-depth analysis of the L2 and L3 calibration algorithms and their validation, including over land.

3.4 Noise mitigation

KaRIn's precision has improved over conventional radar altimetry by more than an order of magnitude (Fu et al., 2024), but SSH derivatives quickly amplify the millimeter-scale noise to the point where it can become the primary limiting factor (Chelton et al., 2022). This is clearly visible in the upper panels of Fig. 10 in the Gulf Stream region. For this reason, Tréboutte et al. (2023) have developed a noise-mitigation algorithm based on a convolutional neural network (CNN) that was specifically trained with SWOT-simulated data in order to reduce random noise while leaving most of the signal intact. In essence, the CNN is able to discriminate between decorrelated random noise and geographically correlated ocean features. In simulations, this strategy performs better than kernel filters or the variational filter from Gómez-Navarro et al. (2020).

Nevertheless, the prelaunch CNN did not work as expected on SWOT's flight data for two reasons. Firstly, the noise floor of the flight data is significantly better than in simulations, as well as being more correlated at 2 km than the pure white noise they used in simulations. Secondly, KaRIn flight data have a series of outlier and correlated glitches as well as some ocean features that were not in the prelaunch simulated training dataset: e.g., rain cells that are not edited, spurious pixels from the coast or sea ice, and strong nonlinear internal waves. The prelaunch CNN generally behaved poorly when it encountered features such as these that it was not trained on.

[6]The large difference between the two orbits is discussed by Dibarboure et al. (2022) and is beyond the scope of this paper. In essence, the 1 d phase has very few crossovers because of the sparse geographical coverage, which in turn thresholds the Level-2 calibration, which is based on crossover overlaps. The Level-3 algorithm leverages multiple nadir altimeter missions, which makes it much more resilient to this SWOT crossover sparsity.

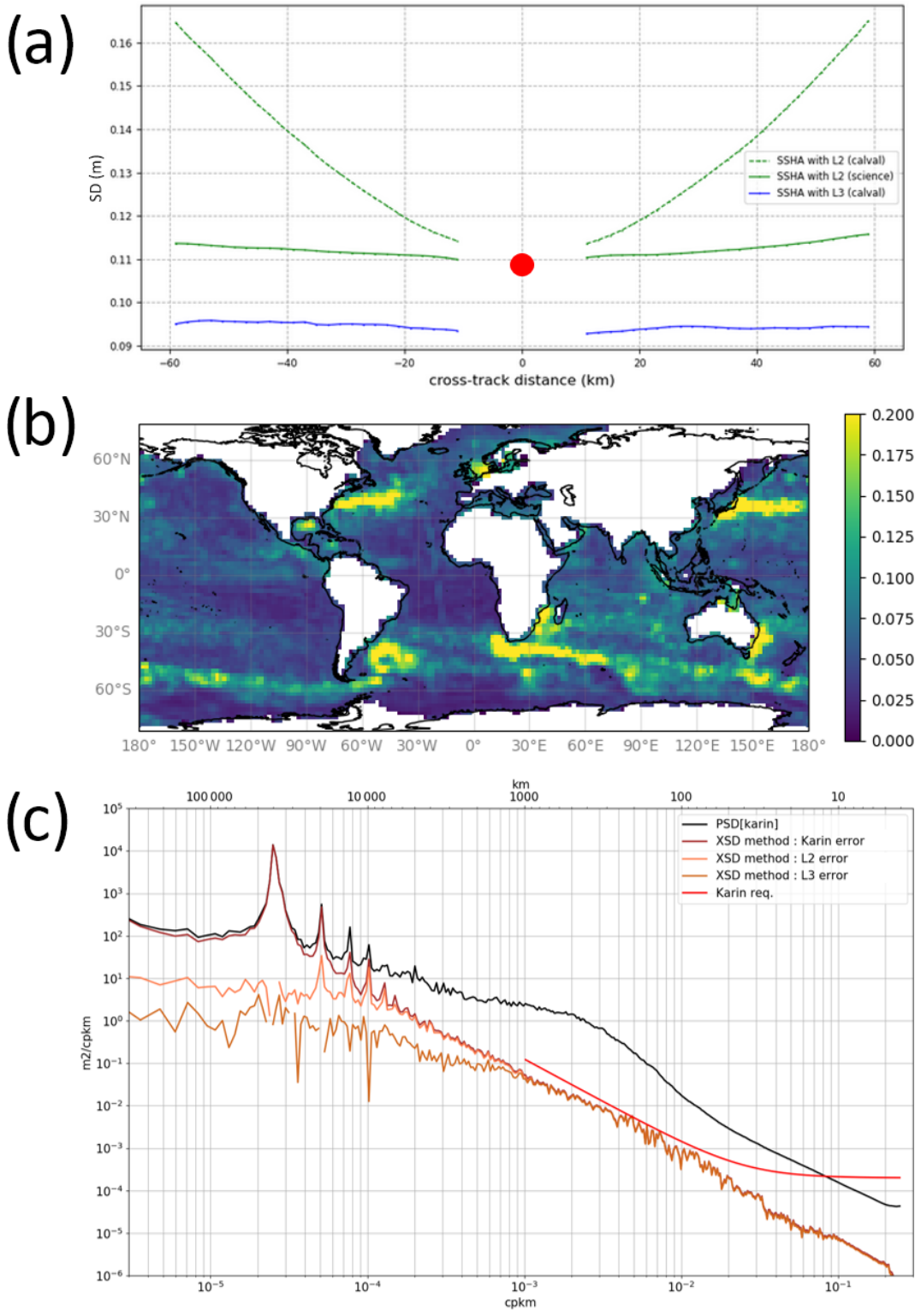

Figure 9. The reduction in KaRIn's systematic errors with the data-driven calibration. Panel **(a)** shows the variance in the KaRIn SSHA as a function of the cross-track distance. The dotted green curve is after the Level-2 calibration for the 1 d orbit, and the plain green curve is for the 21 d orbit. The blue curve is after the Level-3 calibration. The red dot is the variance in the nadir altimeter SSHA for the 21 d orbit. Panel **(b)** is a map of the KaRIn SSHA standard deviation (in cm). Panel **(c)** is the power spectrum of the KaRIn SSHA (black) and an estimate of the KaRIn systematic errors ($B/L/Q$ components) before calibration (dark brown), after Level-2 calibration (orange), and after Level-3 calibration (light brown). The KaRIn ocean requirements are also shown in red.

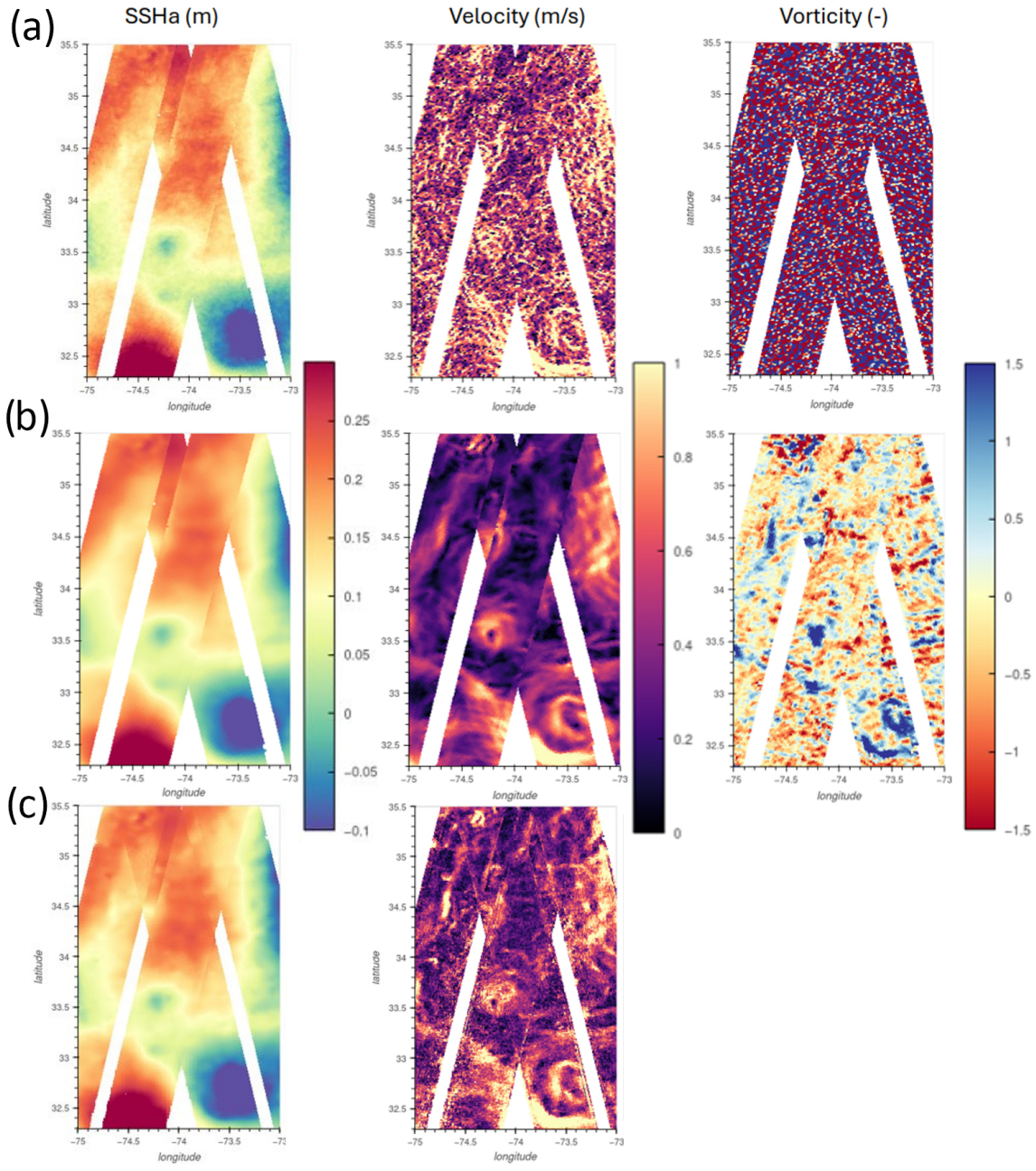

Figure 10. An example of 2 km KaRIn SSHA before **(a)** and after (**b** and **c**) denoising in the Gulf Stream (May 2023). From left to right: sea surface height anomaly, geostrophic velocity, and relative vorticity. The panels in **(b)** are from the 2 km product, and the panels in **(c)** are from the 250 m product. Note that the 250 m geostrophic velocities before denoising are barely usable (dominated by random noise with a magnitude much higher than 1 m s^{-1}).

So the same CNN (UNet variant) was retrained on a more realistic training dataset with less random noise than in prelaunch simulations and with training on the eNATL60 model with tides (Ajayi et al., 2020; Brodeau et al., 2020) to better simulate the SWOT observations. The retraining was performed with random-wave-modulated white noise at 250 m, with a Hamming filter to mimic the downscaling to 2 km that is performed in the ground segment. Lastly, in order to generate as realistic as possible a training dataset, we used the style transfer technique from Gatys et al. (2016): we used the simulated SWOT product as the first input and real SWOT images to define the target style. This approach yields a training dataset that is more realistic, with more diverse oceanic and atmospheric conditions. This retraining improved the denoising behavior in most places.

Some denoising examples are shown in Fig. 10: the upper panels are the SSHA and some derivatives from the original SWOT images (2 km resolution), while the lower panels are the same scene after denoising by the UNet. In the Gulf Stream region, the UNet is able to take out most of the noise in geostrophic velocities without a massive smoothing of oceanic features as small as 10 to 20 km. Moreover, it seems to retrieve some vorticity features. Although the latter remain quite noisy, the UNet does yield a massive improvement upon the original vorticity (upper-right panel). In this example, a traditional kernel smoother would essentially smooth out most if not all small-scale features of second derivatives (Chelton et al., 2022). In the 250 m example in Fig. 10c, the geostrophic velocities are computed on a nine-point stencil in the same way as for the 2 km counterpart. This results in more noisy gradients since they are effectively computed with a distance 8 times shorter than in Fig. 10b. Still, the bottom-right panels of Fig. 10 show that the 250 m product is consistent with its 2 km counterpart, and it can retrieve even smaller features or sharper gradients. This might prove beneficial for some specific users, such as geodesists that want to leverage the SSH slope to derive gravity anomalies and bathymetry (e.g., Yu et al., 2024).

On average, the UNet removes approximately 5 mm rms from the SSHA. These values were found to be stable over a few months of the science orbit. KaRIn's noise floor is arguably closer to a couple of mm rms, so the filter is probably removing more than just the random noise from KaRIn: it takes out either some ocean features or some correlated errors from KaRIn. This is confirmed by the PSD of Fig. 12a. Before denoising (blue curve), the SSHA spectrum exhibits a spectral slope transition from $K^{-3.5}$ (or $K^{-11/3}$) for the larger mesoscale to K^{-2} below 70 km. This slope break might originate from unbalanced motion (internal tides, internal waves) or from red-colored KaRIn measurement errors (e.g., from atmospheric or sea-state sources). In contrast, after the L3 denoising (orange curve) the SSHA spectrum is linear from the larger scales to 15 km. In other words, the denoising seem to mitigate not just random white noise but also a fraction of the K^{-2} slope break below 70 km. The PSD of the UNet residual (green curve) more or less follows a $K^{-0.5}$ slope. In other words, the UNet might be capturing either red-colored KaRIn errors (e.g., wet troposphere, atmosphere, or rain or sea-state residuals) or ocean features in addition to instrumental random noise.

Furthermore, some properties of the noise content can inferred from the spectra of similar plots for 24 h differences[7] during the 1 d phase of SWOT (Fig. 12b). Before denoising (blue curve), a large fraction of the large mesoscale is canceled out in 24 h (as expected). In contrast, the linear part below 100 km is barely removed by the 24 h difference; i.e., the K^{-2} slope discussed above is mostly decorrelated in 24 h, especially at the smallest scales. After denoising (orange curve), the 24 h differences are mostly the same for the larger scales, but the linear trend is removed: the 24 h difference PSD (plain orange line) slowly converges towards the PSD of the denoised SSHA. This is what one would expect from a PSD dominated by ocean mesoscale features, where the shorter wavelengths also decorrelate faster in time. The spectrum of the 24 h difference in the UNet residual (plain green line) is also very close to the mean PSD of this residual (dashed green line), which indicates that the content removed by the UNet is decorrelated in 24 h (as one would expect from measurement errors, atmospheric and sea-state effects, or internal waves). But the two green curves are not perfectly aligned, and approximately 30 % of the variance is missing: the UNet has either captured some temporally coherent errors (unlikely for atmospheric, sea-state, or random errors) or absorbed a small fraction of temporally coherent ocean features (e.g., higher modes of internal tides or a small fraction of the stationary mesoscale).

Note that we do not have any ground truth to quantify the denoising performance. Thus it is difficult to determine if the noise mitigation has only positive effects or if the smaller features in the SSHA derivatives are also made of correlated noise. From the day-to-day consistency that we observe in subsequent images of the CalVal (calibration–validation) phase, we think there is desirable noise-mitigation skill in the current combination. However, that statement is subjective and is by no means a proper demonstration. The spectra of Fig. 12 are consistent with what one might expect from denoising, but we cannot rule out the possibility that the UNet is inventing or distorting some features to replicate the properties of its training dataset.

Therefore, the noise-mitigated SSHA is provided as an optional asset of the Level-3 products: in the basic L3 variant, it is provided in addition to the original raw/unfiltered SSHA. In the expert variant, it is provided as a separate optional layer that can be ignored.

3.5 Topography derivatives

The Level-3 products from KaRIn also include geostrophic velocities and relative vorticity in 2D. This is a relatively simple addition provided only for the sake of user convenience. As explained in the previous section, the derivatives are computed based on the noise-mitigated SSHA only. The differentiation is computed with a nine-point stencil, following the methodology of Arbic et al. (2012). The rationale is to minimize velocity-dependent biases. The stencils were originally developed for very coarse Level-4 altimetry maps (also known as AVISO maps), but Arbic et al. (2012) show that a 5 km resolution model still benefits from larger stencils.

[7] A factor of $1/2$ is applied to the PSD of 24 h differences. The rationale is that if a given random signal S is decorrelated in 24 h, the PSD (or variance) of the 24 h difference $S_d - S_{d+1}$ will be equal to twice the PSD (or variance) of S because the co-spectrum (or covariance) is zero. The factor $1/2$ will then realign the PSD of $S_d - S_{d+1}$ with the PSD of S_d and S_{d+1}.

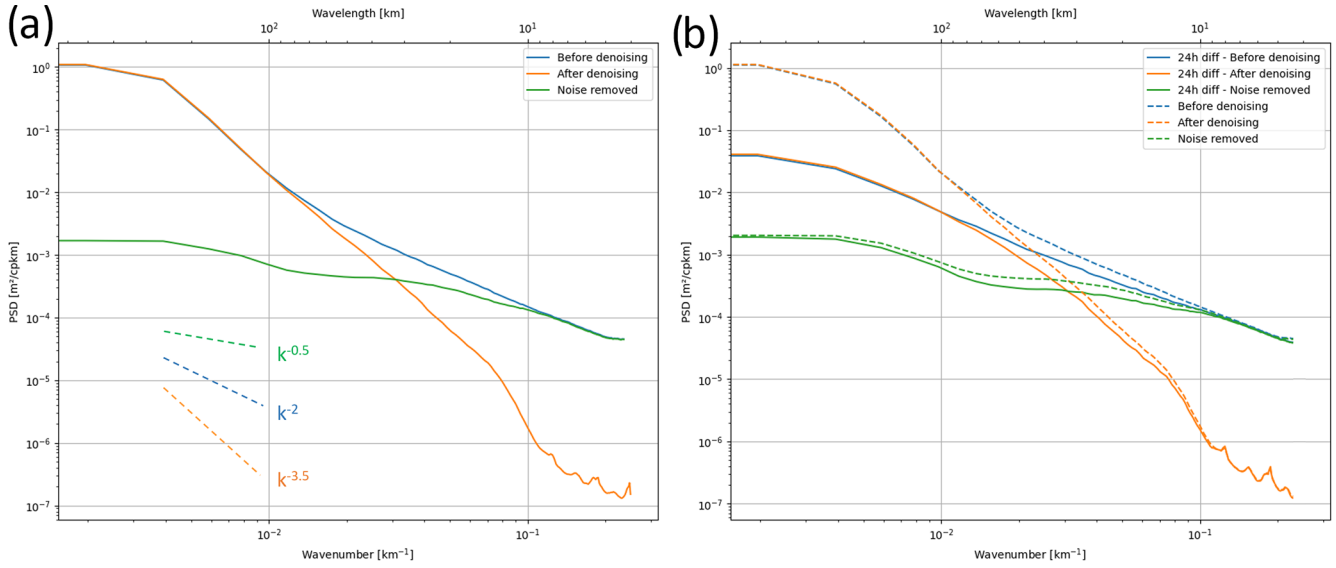

Figure 11. PSD of the KaRIn SSHA (in $m^2\,cpkm^{-1}$, cycles per kilometer). The blue curve is before our L3 denoising. The orange curve is after the UNet is used. The green curve is the PSD of the noise removed by the UNet. Panel **(a)** is for the SSHA itself. Panel **(b)** is the same but with the addition of 24 h differences from the 1 d phase (plain lines).

4 Level-3 product validation and use cases

The SWOT interferometer is the first instrument of its kind; its validation is still ongoing. At the time of writing, there is no public dataset able to provide a solid ground truth to evaluate the benefits of the Level-3 algorithms presented above. In previous sections, we illustrated and quantified how each layer of the Level-3 algorithm brought a small improvement to the overall product. In this section, we analyze the complete Level-3 product.

In Sect. 4.1, we provide a global overview of the product content, as well as some qualitative internal and multi-sensor comparisons. Then in Sect. 4.2, we quantify the differences between SWOT and Sentinel-3 (the operational altimeter from the European program Copernicus) for Level-2 and Level-3 products.

4.1 Qualitative assessment

For a qualitative point of view, a gallery of examples of the Level-3 product from KaRIn is given in Fig. 13. The global map is a composite of one cycle of a 21 d orbit in November 2023. The panels below the global map are a series of regional zooms of the global map to highlight different recurring features that may be seen in KaRIn images. For the global ocean, the SSHA is strikingly consistent with gridded Level-4 products from Copernicus Marine Service (sometimes referred to as AVISO maps), although for SWOT KaRIn, no interpolation is needed. KaRIn alone is able to cover most of the ocean a couple of times every 21 d (ascending and descending passes).

The large scale of the Level-3 product is very consistent once it is calibrated: e.g., the Indian Dipole in a positive phase (Fig. 13a) or the El Niño event of fall 2023 (Fig. 13e). Even at these larger scales, the Level-3 product is better than the Level-2 one because of the newer tidal model and the multi-mission data-driven calibration.

Incidentally, a series of vertical stripes can be found in various regions (e.g., Fig. 13d). This pattern is expected from such SWOT composites: it originates in the stroboscopic sampling pattern of the SWOT orbit. Indeed, the global coverage of SWOT's 21 d orbit is assembled from two subcycles of 10.5 d each (Lamy and Albouys, 2014). Each subcycle of 10.5 d corresponds to a global coverage pattern that is interwoven (in longitude) with the coverage of the previous and following subcycles. In other words, with every half cycle, SWOT covers half of the ocean, alternating between two interwoven scan patterns. Furthermore, the El Niño event quickly propagates eastwards over a 10 d period, and the stripes indicate that the SSHA is rapidly evolving between subsequent interwoven scans from SWOT. For the same reasons, stripe-shaped discrepancies can be found between adjoining swaths in all regions where the ocean changes significantly faster than the 10.5 d it takes to get the interwoven scan.

Moreover, KaRIn provides a consistent view of mesoscale eddies in the Southern Ocean (e.g., Fig. 13g). The larger mesoscale (150 km or more) is relatively well-known from nadir altimetry Level-4 maps, i.e., after an interpolation of many 1D profiles spanning tens of days. In contrast, the Level-3 product from SWOT provides a synoptic view of the larger mesoscale without any interpolation whatsoever:

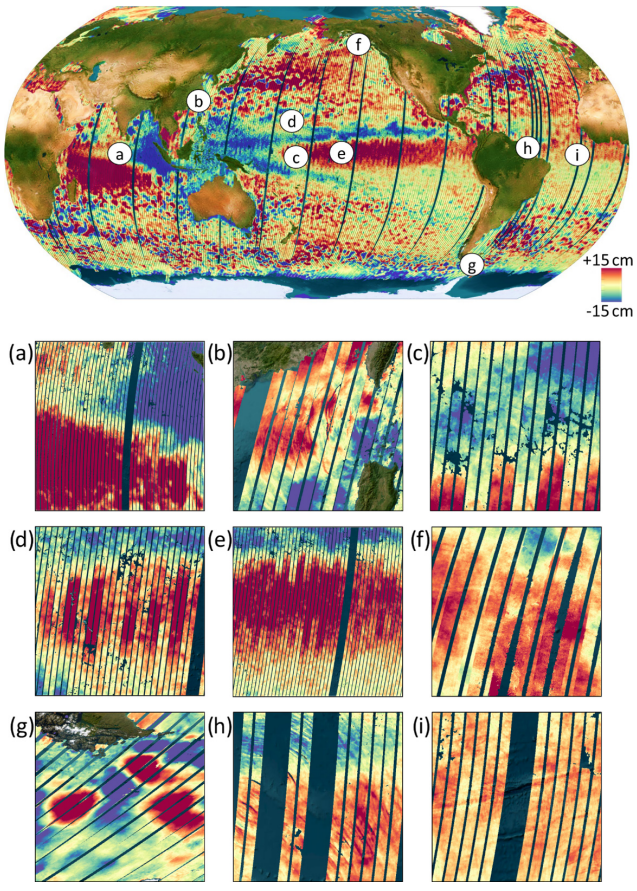

Figure 12. Example of a Level-3 SSHA composite (in cm) for November 2023 (ascending passes). Panels **(a)** to **(i)** are regional zooms from the global map.

it captures the actual shape and amplitude of each eddy without the distortion and smoothing that one might expect from the gridding procedure of Level-4 products. Furthermore, in addition to the larger mesoscale, medium to small to submesoscale are also retrieved in Level-3 products. Figure 13g contains some eddies as small as 20 to 50 km. These features are beyond the resolving capabilities of 1D altimetry (Ballarotta et al., 2019) for two reasons: (1) the constellation of four to seven nadir altimeters does not have enough coverage to resolve these features in space and time and (2) the precision of 1D altimeters is, on average, insufficient to consistently observe them in 1D segments. Therefore, KaRIn is major breakthrough in the observation of smaller ocean turbulence (Fu et al., 2024). Note that these eddies near Drake Passage in Fig. 13g appear quite consistent between neighboring swaths. This highlights a remarkable feature of the SWOT subcycles: the ascending passes shown here from one 10.5 d subcycle are laid down over consecutive days towards the west. At middle to high latitudes as the swaths converge, this allows a consistent composite 2D local sampling 600 km wide over 5 d, with only 1 d offsets between neighboring tracks. Then the SWOT descending passes form another 5 d local 600 km wide sampling, which is repeated in the second 10.5 d subcycle. The largest eddies are clearly visible in the SSHA, and geostrophic velocities and are generally quite consistent over neighboring passes: any discrepancy between adjoining passes clearly outlines how fast eddies are moving in a few days.

The self-consistency and the occasional discrepancies induced by the 10.5 d scanning pattern are also visible in SSHA derivatives (Fig. 14 for the North Atlantic Ocean and the Gulf Stream region). However, there are two noteworthy features of the geostrophic velocities in Fig. 13 that deserve a more thorough analysis: (1) there are many filament-like features in the open ocean (far fewer over the continental shelf) that could be due to background-correlated noise and (2) in the southeastern part of the maps, some stripe-shaped SSHA features are interpreted as geostrophic velocities. These patterns, also clearly visible in the western tropical Atlantic (Fig. 13h) or in the Luzon Strait (Fig. 13b), are actually caused by internal tides or solitons and not by mesoscale dynamics. KaRIn gives a single synoptic view of the scene, and although a coherent internal tidal model correction has been applied for the SSHA, this model is not perfect and cannot correct for incoherent, non-phase-locked internal tides or solitons. As a result, the SSHA still contains the signature of unbalanced motion and waves. When these waves are close to their generation sites, they are coherent and structured and therefore clearly visible. However, once they interact with mesoscale of the same size and amplitude, it might become a lot more difficult to separate balanced and unbalanced motions from a single Level-3 product. This topic is quite complex and is beyond the scope of this paper, but Figs. 13 and 14 illustrate the complexity of quantitative validation of SSHA without a global ground truth and show that care must be taken when interpreting geostrophic velocities since many SSHA features captured by SWOT are not in geostrophic balance.

In order to confirm the presence of small mesoscale features seen by KaRIn, we compared SWOT's geostrophic velocities and ocean color images for a series of cloudless days. In the example from Fig. 14, the largest eddies (more than 150 km) are very consistent, as expected, and the smaller ones illustrate quite well that SWOT-derived velocities provide a synoptic view of the dominating factor for the ocean color advection in this region. This is particularly interesting for thin fronts and eddies of a few tens of kilometers. While both variables are not expected to be fully consistent at all times, this qualitative comparison shows a good qualitative correlation: our Level-3 product is a good asset for multi-sensor comparisons. At these scales, the Level-3 product is better than the Level-2 one because of the MSS and MDT models, the calibrated-phase screen, and better editing of spurious pixels.

A different approach to verify the qualitative consistency of the Level-3 product is shown for two arbitrary exam-

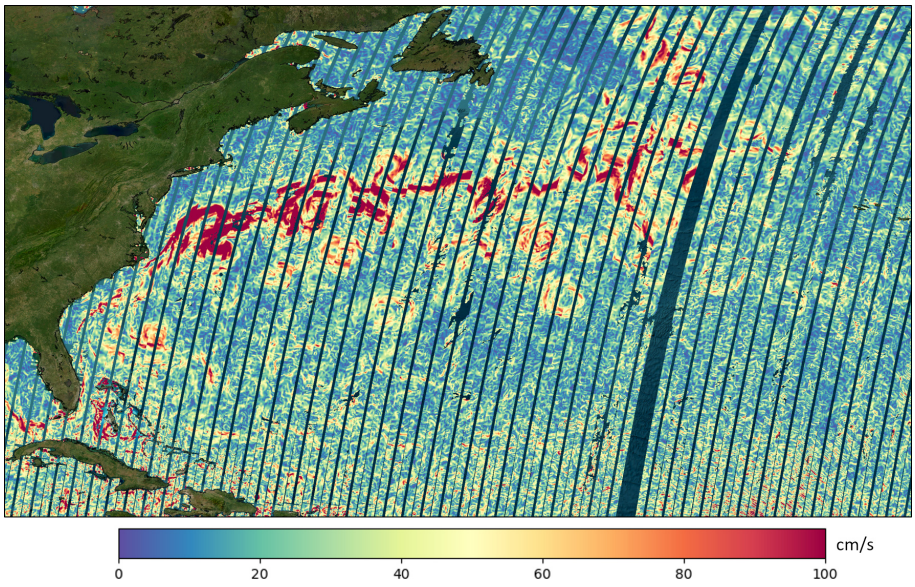

Figure 13. Geostrophic velocities derived from the KaRIn SSHA for the North Atlantic region.

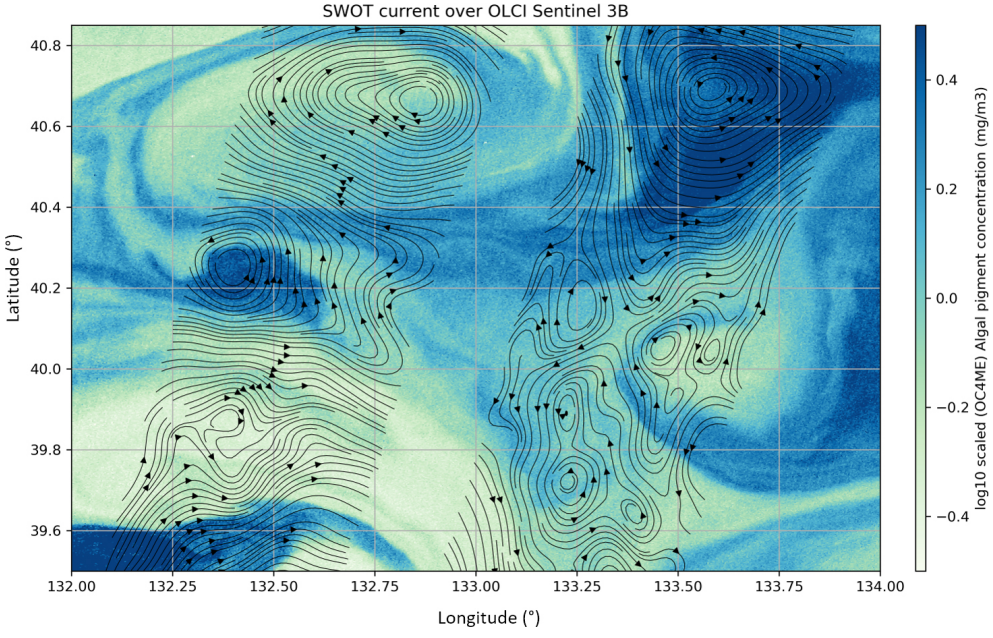

Figure 14. Comparison between the Sentinel-3/OLCI sensor and SWOT KaRIn for 11 May 2023 in the Sea of Japan (East Sea). The background image is the chlorophyll OC4ME product from Copernicus Marine Service. The black lines are streamlines derived from the SWOT/KaRIn geostrophic velocities (two swaths of 50 km each).

ples in Fig. 15. Here, we use the short temporal revisit of the 1 d phase to analyze the evolution of various mesoscale features in western boundary currents. Firstly, the comparison confirms the self-consistency of SWOT over subsequent days and different measurement conditions. Indeed, panels (a) and (b) are very consistent, and the difference (panel c) is small in comparison, despite major changes in the atmosphere and sea-state conditions (more than 5 m) in 4 d. More importantly, the rms of the KaRIn/KaRIn differences in panel (c) exhibits a well-behaved PDF (not shown) and a variance of 1 cm^2, i.e., much less than the nadir/nadir differences (3 cm^2). The Southern Ocean is an interesting region for this qualitative validation exercise, especially over slow-moving or bathymetry-trapped eddies: their stability is a good way to confirm the repeating nature of KaRIn SSHA in different atmosphere and/or sea-state conditions. Secondly, in various

cases (e.g., Fig. 15d and e), the consistency between SWOT Level-3 products (both sensors) and the nadir altimetry constellation remains good, but the temporal smoothing of the 2D nadir maps can limit their ability to serve as a ground truth for KaRIn validation. Indeed, the eddies from panels (d) to (f) are moving very fast, and the 1D altimeter constellation underestimates their deformation and actual shape. However, it does provide a trustworthy albeit blurry view of the mesoscale field to help determine if the changes in KaRIn images are happening or not.

In the Kuroshio example (Fig. 15d to f), SWOT observes a consistent and rapid change: the bigger eddies are not only traveling faster than the interpolated Level-4 map might indicate, but their shape is anisotropic and is evolving very quickly as the four eddies in the SWOT scene interact with one another. Panel (f) also shows that in 4 d, the SSHA changes by 30 cm or more at the heart of the interaction. This is significantly more intense and faster than what is usually observed by Level-4 products from nadir altimetry because the temporal resolution of this product is more than 2 weeks (Ballarotta et al., 2019).

More importantly for the Level-3 validation, this example from the 1 d phase captures the temporal evolution of the KaRIn product that seems intuitive and reasonably robust. We do lose small image fragments due to rain in panels (e) and (f), and some artifacts may remain, but the Level-3 product captures the temporal evolution of the mesoscale during the 1 d phase.

Lastly, some limits of the SWOT/KaRIn products are visible in Fig. 13. In panel (c), many parts of the images are missing. This is caused by tropical rain events that are edited out when the SSHA is not usable (see Sect. 3.2). In panel (f), some swaths have a lot of visible noise. This is caused by the presence of a major storm and high waves (typically 6 m or more): in these conditions, KaRIn images become a lot noisier even at this 2 km resolution (Peral et al., 2024), albeit much less than the profiles of traditional altimeters. Note that the noisy image segments remain usable: the coverage remains good, and the larger scales are not significantly degraded.

4.2 Comparison with external altimeters

In order to quantify the residual errors from our KaRIn product, we computed all crossover sections with altimeter profiles from Sentinel-3A and 3B with a time difference less than 24 h. When the solar time of SWOT is aligned with the sun-synchronous orbit of Sentinel-3 (S3), there are thousands of crossover matchups where S3 passes through the KaRIn swath, thus creating millions of pixel associations between both sensors. Moreover, when the S3 nadir profile crosses the SWOT nadir profile, we also get nadir/nadir altimeter crossover points. More importantly, because SWOT does not use a sun-synchronous orbit, the crossover matchups will migrate in space and cover all regions in a semi-systematic pattern. This provides homogeneous coverage of the global ocean. Over these matchups, we can use the SSHA difference between SWOT and S3 to infer how much error might be affecting our Level-3 product.

This is not trivial because the time difference between both measurements is not zero and because Sentinel-3 has its own error sources. Dibarboure and Morrow (2016) performed a similar exercise with the geodetic phase of Jason-1, when the longitude-drifting tracks of Jason-1 align with the tracks of Jason-2. They used these long alignments of nadir tracks to quantify the variance, geographical distribution, and power spectra of the SSHA difference for 24 h or less. To illustrate, they find a variance on the order of 3 cm rms for 0 d differences (essentially the random error in both altimeters – 2.7 cm rms each), which increases rapidly to 4 cm rms if the time difference is 24 h or less (i.e., +3 cm rms from the 24 h ocean variability).

The differences between $\mathrm{SWOT_{nadir}}$ or $\mathrm{SWOT_{KaRIn}}$ and S3A or S3B all exhibit a PDF that is well-behaved[8] (Fig. 16a): the mean of the SWOT/S3 differences for L2 products is almost but not exactly zero. S3B crossovers exhibit a small bias of the order of 6 or 7 mm (seen by $\mathrm{SWOT_{nadir}}$ and $\mathrm{SWOT_{KaRIn}}$), and $\mathrm{SWOT_{KaRIn}}$ crossovers exhibit a bias of 1 or 2 mm with respect to $\mathrm{SWOT_{nadir}}$ crossovers. The standard deviation (SD) of these 24 h crossover differences is approximately 5.4 cm for both SWOT instruments. In other words, the nadir altimeters of SWOT and KaRIn exhibit similar errors, and SWOT has slightly less (relative) bias than Sentinel-3B.

If we use the results from Dibarboure and Morrow (2016) to account for the known variance in Sentinel-3 errors and 24 h ocean variability, we obtain a residual on the order of 3.3 cm rms for both sensors of SWOT (unexplained variance that might be interpreted as SWOT error). For the nadir altimeter, this number is consistent with its theoretical error budget (all SSHA components, including residual errors from geophysical corrections and models), so we can assume that this metric is also a good ballpark estimate of the total KaRIn error in the Level-2 products.

Discussing the details of each component in the SSHA error budget (SWOT, 2024) is beyond the scope of this paper, as their total error budget includes many components: e.g., precise orbit determination error, random noise, the wet and dry troposphere, ionosphere and sea-state bias, and residuals from the data-driven calibration. Yet some of these contributors are the same for both sensors (e.g., orbit determination or geophysical models), while others are not. The two

[8]The KaRIn/nadir PDF is smoother than the nadir/nadir one. This is because each $\mathrm{SWOT_{KaRIn}}$ crossover segment yields 50–200 times more pixel matchups than $\mathrm{SWOT_{nadir}}$ crossover points. A $\mathrm{SWOT_{KaRIn}}$/S3 crossover segment can be as long as thousands of kilometers when the SWOT/S3 solar times are aligned.

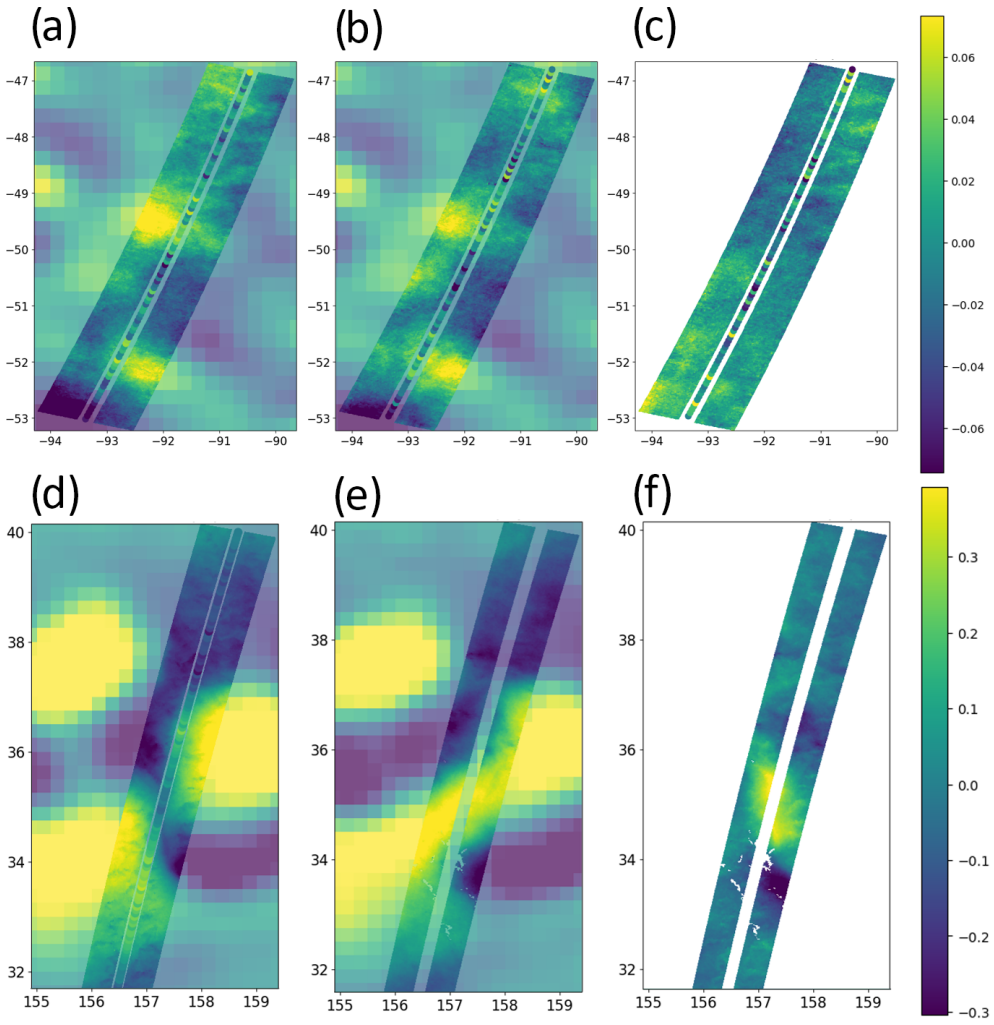

Figure 15. Consistency of the Level-3 product in time in the Southern Ocean **(a–c)** and in the Kuroshio region **(d–f)**. Panels **(a)** and **(d)** show an arbitrary KaRIn swath during the 1 d phase of SWOT. The KaRIn image is shown on top of the Level-4 maps from Copernicus Marine Service (pixelated background, same color scale). Panels **(b)** and **(e)** are the same regions 4 d later. Panels **(c)** and **(f)** are the differences between the left and right columns.

main differences are the long-wavelength errors and random noise[9].

Indeed, KaRIn has much less random noise than a nadir altimeter, but it has additional sources of error that do not exist in nadir altimetry. In particular, the systematic errors (e.g., uncorrected satellite roll, interferometric-phase bias) are mitigated by the data-driven calibration (discussed in Sect. 3.3). This error source has a variance that increases as a function of the cross-track distance with linear and quadratic amplitude (i.e., x^2 or x^4 in variance). Conversely, for the global ocean and the science orbit, the geophysical SSHA variance has no reason to be different in the nadir, near-range, or far-range areas. In other words, a perfectly calibrated SSHA would yield a flat curve as a function of the cross-track distance in Fig. 16b: the parabolic shape of the variance as a function of the cross-track in Fig. 16b is a clear indicator of residual systematic errors that have not been fully calibrated in the L2 product. The error variance that increases in the cross-track direction can be attributed to calibration residuals (2.2 cm rms[10]), and the background variance at the nadir point can be attributed to all other sources of KaRIn error (3.1 cm rms[11]).

[9]There is also a third difference in the ionosphere error. KaRIn is in the Ka-band and is therefore 7 times less sensitive to ionosphere errors, while the SWOT and S3 nadir altimeters are in the Ku/C bands and use a filtered dual-frequency ionosphere correction. As a result, the ionosphere is a small contributor to the S3/SWOT differences. We will make the approximation that it can be ignored.

[10]The variance increases from 27.5 cm^2 at the nadir point to 32.5 cm^2 on average in the swath (i.e., 5 cm^2 or 2.2 cm rms).

[11]The variance at the nadir point is 27.5 cm^2 or 5.4 cm rms. We interpolate the U-shaped curves of KaRIn. Approximately 3 cm rms

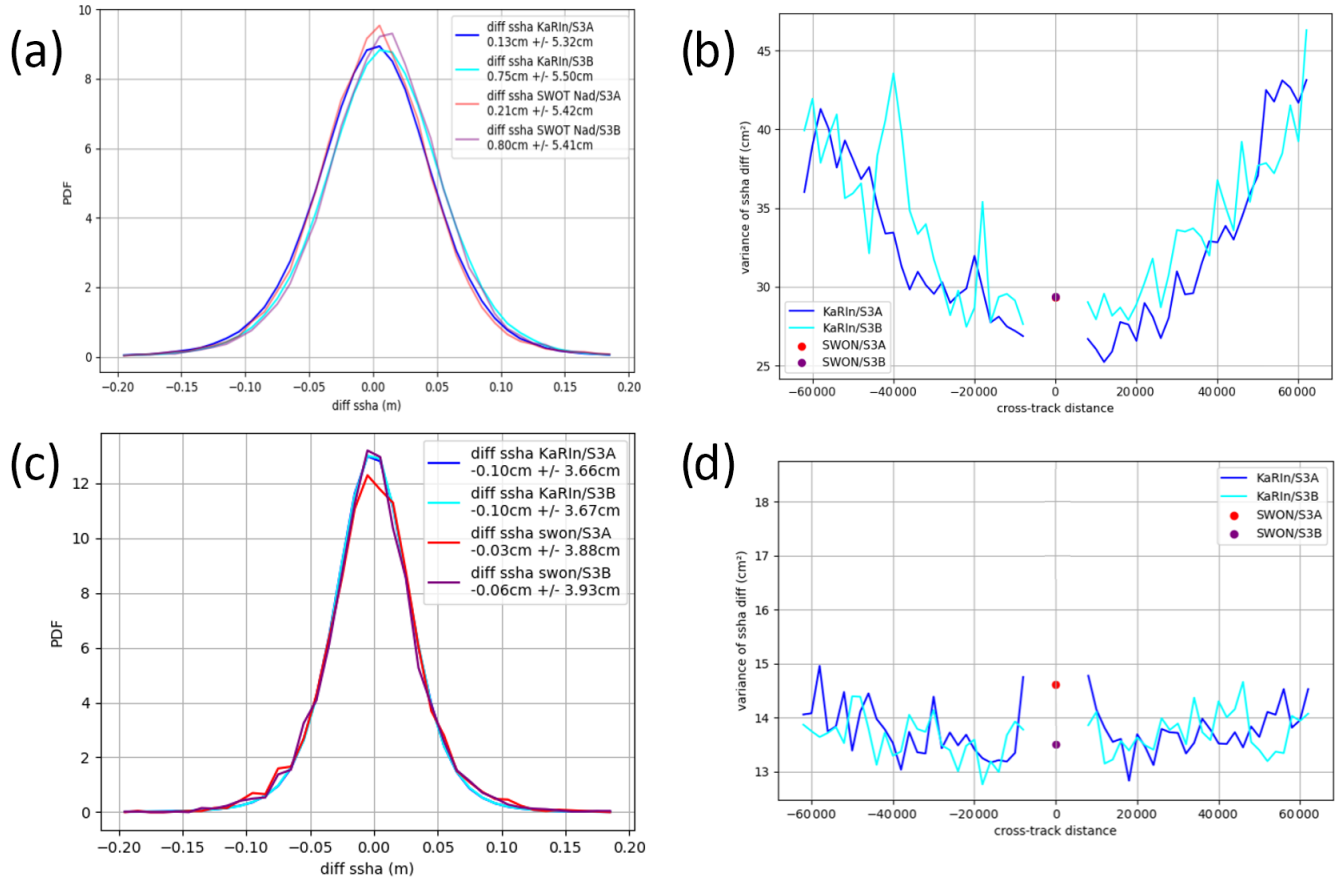

Figure 16. Statistics of the crossover differences between the SWOT SSHA and the Sentinel-3 SSHA for the Level-2 products **(a, b)** and the Level-3 products **(c, d)**. Panels **(a)** and **(c)** are the probability distribution functions of the SSHA difference. Panels **(b)** and **(d)** are the variance in the SSHA difference as a function of the cross-track distance. Dark blue is for SWOT/KaRIn and Sentinel-3A. Light blue is for SWOT/KaRIn and Sentinel-3B. Red is for SWOT/nadir altimeter and Sentinel-3A. Purple is for SWOT/nadir altimeter and Sentinel-3B. The crossover time difference is 24 h or less.

A similar comparison of the Level-3 products of SWOT and Sentinel-3 shows that the L3 calibration has significantly improved the consistency with Sentinel-3 for both SWOT instruments (Fig. 16c and d). This is expected: for nadir altimeters, multi-mission calibration is known to reduce precise orbit determination (POD) error, as well as reduce residuals from barotropic corrections and instrument and processing biases (Dibarboure et al., 2011). The benefits are the same for KaRIn since the Level-2 sources of errors are the same. In addition, the L3 data-driven calibration mitigates the KaRIn-specific systematic errors better (e.g., spacecraft roll), thanks to multi-mission crossovers.

The resulting PDF of the SSHA crossover difference is still well-behaved (Fig. 16c), and there is a bias of only a couple of millimeters and an SD of 3.9 cm for $\mathrm{SWOT}_{\mathrm{nadir}}$ and 3.7 cm for $\mathrm{SWOT}_{\mathrm{KaRIn}}$. Contrary to the errors observed in L2 products, here KaRIn exhibits less error than the SWOT nadir altimeter (−1.2 cm rms): this is because the L3 algorithm reduced POD or tide/DAC (dynamic atmospheric correction) residuals for both instruments, and the L3 calibration also removed a bigger fraction of KaRIn's systematic error. Furthermore, Fig. 16d exhibits barely any quadratic shape in the cross-track direction: the error is slightly higher on the edges of each swath, by less than 1 cm rms, which indicates that the L and Q components have been reduced to a residual that is barely measurable. If we account for the S3 error budget and natural variability in the SWOT/S3 24 h difference, this leaves approximately 1.8 cm rms of other error sources in the L3 product (e.g., POD, geophysical corrections including tides and atmospheric correction, noise, and biases of all sorts).

To summarize, the sum of all KaRIn Level-2 errors (including calibration residuals and geophysical corrections) are on the same order of magnitude as the total error in the Level-2 nadir altimeter. However, the nature of this error is differ-

or 9 cm^2 can be attributed to S3A and S3B (S3 error budget document) and 9 cm^2 to the 24 h ocean variability according to Dibarboure and Morrow (2016). The difference yields approximately 9.5 cm^2 or 3.1 cm rms for other error sources, including tidal models or high-frequency barotropic motion caused by the atmosphere.

ent: the nadir altimeter has more random noise, while the KaRIn interferometer is more affected by long-wavelength calibration residuals. In the L3 products, the total error in both instruments is reduced by the multi-mission calibration scheme. And because the KaRIn total error is dominated by L2 calibration residuals that are better calibrated with the L3 multi-mission algorithm, the error in the KaRIn L3 product becomes smaller than in the nadir counterpart.

Furthermore, Fig. 17 gives some insights into the geographical distribution of the error:

- The left panels (a to c) show the mean of the KaRIn/S3 difference.
- The right panels (d to f) show the variance in the KaRIn/S3 difference.
- The upper panels are based on Level-2 products for both missions. This plot measures the discrepancies between Level-2 products before any Level-3 algorithm is used. The two datasets are completely independent.
- The center panels are based on Level-2 products for SWOT and Level-3 products for S3. At this point, SWOT and S3 are still completely independent. Therefore, if the consistency with the SWOT Level-2 product is improved, it means that the nadir L3 calibration of Sentinel-3 reduced some long-wavelengths errors that are specific to this mission (as expected).
- Lastly, the bottom panels are based on Level-3 products for both missions. Here, both S3 and SWOT are input into the SWOT L3 processor, and the two missions are no longer independent. By construction, the L3 process reduces the discrepancies between SWOT, S3, and the rest of the constellation. These panels do not capture the SWOT error since both missions might have common errors (e.g., inherited from the reference altimeter Sentinel-6). Nevertheless, these panels gauge whether SWOT is properly blended in the altimeter constellation.

Although the global bias between SWOT and S3 was very small in Fig. 16, regional biases can be as large as a few centimeters in the eastern Pacific Ocean and the Indian Ocean (Fig. 17a; 60–120° W and 60–120° E, respectively). Such a dipole could originate from small POD residuals. Moreover, calibrating Sentinel-3A and B with the L3 nadir multi-mission processing (independent from SWOT data) tends to reduce the regional bias in KaRIn (Fig. 17b). In other words, the bulk of regional biases from panel (a) is likely caused by S3 rather than by SWOT. Lastly, as expected from the multi-mission approach, when the Level-3 calibration is applied to both S3 and KaRIn, the bias is negligible almost everywhere (Fig. 17c).

Similarly, in the Level-2 products, the variance is rather homogeneous in the open ocean and is slightly higher over the continental shelf and at higher latitudes and some latitude bands (Fig. 17d). In contrast, the calibration of S3 (but not SWOT) substantially reduced the error in many regions (Fig. 17e); i.e., a fraction of the variance in panel (d) actually originates in Sentinel-3 and not in SWOT. Lastly, for the Level-3 products in panel (f), the variance is no longer homogeneously distributed. The background variance in the open ocean is reduced (by L3 calibration of KaRIn). The continental shelves have much less variance than in panel (d). Firstly, the improved geophysical corrections (see Sect. 3.1 and Appendix A) mitigated the SWOT/S3 standard discrepancy. Secondly, the L3 calibration absorbed a fraction of residual errors from barotropic tide corrections or atmospheric corrections. Moreover, the spurious red pixels on this map mostly disappear (better L3 editing process from Sect. 3.2). The remaining variance in L3 crossovers is correlated with the geographical distribution of tropical rain and the wet troposphere, as well as storm tracks or internal tides. There is also a thin alignment near 65° S, which might be related to the flagging process of sea ice for SWOT. The residual discrepancies between S3 and KaRIn L3 products can be explained by suboptimal geophysical corrections to SWOT, to Sentinel-3, or to both.

To summarize, KaRIn/S3 crossovers illustrate the good consistency between both missions with Level-2 products and the excellent blending after Level-3 algorithms have been performed. On average, KaRIn has slightly fewer errors than SWOT's nadir altimeter in the Level-3 product because of editing, geophysical correction, and data-driven calibration. Still, both sensors from SWOT exhibit an error level on the same order of magnitude, with more random noise for the nadir instrument and more long-wavelengths error for KaRIn (on the order of 2 cm for the L2 product and 1–1.5 cm for the L3 product).

5 Discussion: relevance and limits of this dataset

In this section, we illustrate the utility of our SWOT Level-3 product for different research domains. We also discuss limitations of this dataset and how collaborative improvements with experts in various fields and with the SWOT project might yield better products in the future.

5.1 Global circulation and ocean mesoscale

From the previous sections, it is clear that KaRIn has unprecedented ability to observe large and small mesoscales. The gain in resolution is clearly visible in the Gulf Stream (Fig. 1), and the unique properties of the 1 d orbit coverage can be used to explore rapid changes in the mesoscale field (Fig. 15). Moreover, SWOT is consistent with not only itself but also traditional altimeters at all scales: the 21 d orbit makes it possible to get a synoptic view, ranging from large-

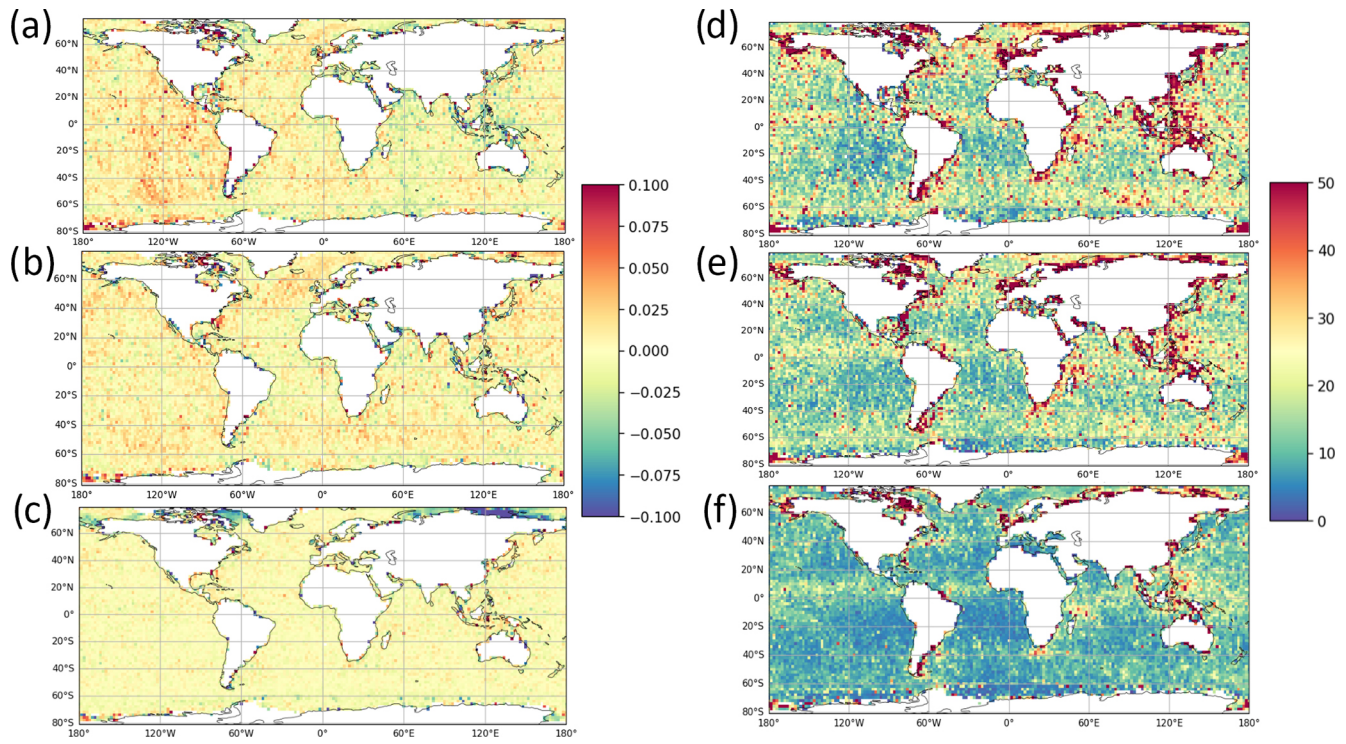

Figure 17. Crossover SSHA differences between KaRIn and Sentinel-3 A and B over November 2023 to February 2024, with crossover time differences of 24 h or less. Panel **(a)** is the mean difference for Level-2 products of both missions (in m). Panel **(b)** is the mean difference for Level-2 KaRIn products and Level-3 Sentinel-3 products from Copernicus Marine Service. Panel **(c)** is the mean difference between our Level-3 KaRIn products and Level-3 Sentinel-3 products from Copernicus Marine Service. Panel **(d)** is the variance in the difference between Level-2 products (in cm^2). Panel **(e)** is the variance in the difference for Level-2 KaRIn products and Level-3 Sentinel-3 products from Copernicus Marine Service. Panel **(f)** is the variance in the difference for Level-3 products.

scale, basin-wide events such as El Niño to the anisotropic structure of small mesoscale eddies (Fig. 12).

This paper has concentrated on the L3 processing of SSHA and its data quality and validation. However, SWOT also has a rich assortment of other 2D observations and derived geophysical parameters that are collocated with L3 SSHA. One key 2D observation is sigma0[12], calculated from the synthetic-aperture radar (SAR) processing of the 2D swath images. Under low-wind and low-wave conditions, it is possible to push KaRIn largely beyond its prelaunch requirements (Fig. 18): panel (a) shows an extremely precise sigma0 from the Level-2 product at 250 m resolution, and panel (b) is our Level-3 SSHA (250 m resolution), with black streamlines from the 2 km geostrophic velocities. In these low-wind and low-wave conditions, panel (a) reveals a wealth of thin oceanic filaments, highlighting the interactions between the surface roughness and the small-scale to submesoscale turbulence, i.e., the KaRIn counterpart of biogenic oil films seen on SAR imagers (e.g., Nichol et al., 2023) and/or the processes described by Rascle et al. (2014).

Although some similar filaments of a small amplitude can be seen in various regions of panel (b), these features are generally (but not always) averaged out at 2 km. The SSHA generally represents mesoscales that are stirring the ocean from depth. In these calm conditions, the SAR sea surface structure is being partially set by the deeper-mesoscale stirring, but the SAR image is capable of detecting the near-surface layer, which clearly evolves with much smaller features. The cause of these thin topography filaments and their correlation with sigma0 images have not been fully described in the literature. They might be real or artifacts. This effect might also exist in nadir altimeters, although if it does, then it is probably hidden by their much larger noise envelope or is simply harder to detect in 1D profiles. This example is one of many observed from SWOT that would clearly benefit from in-depth investigations from submesoscale and sea-state experts and remote sensing experts.

For global ocean circulation and mesoscale studies, the most useful data from both instruments of SWOT are built into the Level-2 products from the SWOT project. Our addi-

[12]The sigma0 of the surface σ_0 is the radar power backscattered by the surface. It is also known as NRCS, or the normalized radar cross-section, in other communities. It essentially provides information on the surface roughness at the radar wavelength scale (i.e., wind and waves in the Ka-band) and/or the effect of atmospheric attenuation (e.g., by rain).

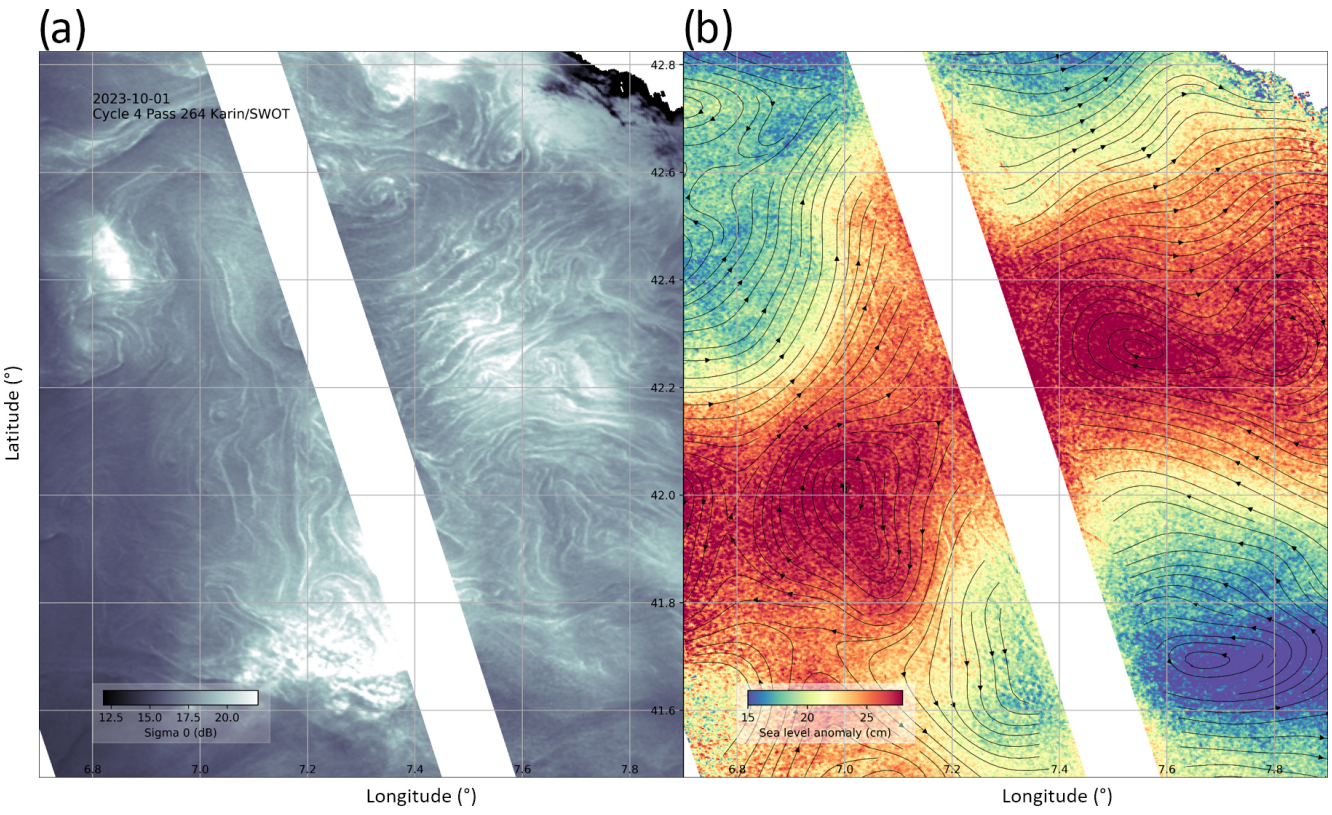

Figure 18. Small to submesoscale turbulence from KaRIn measurements (October 2023, Mediterranean Sea). Panel **(a)** is the sigma0 (in dB) from the Level-2 products. Panel **(b)** is the 250 m SSHA (in cm). The black lines in panel **(b)** are streamlines derived from 2 km geostrophic velocities.

tions to the Level-3 layers help reduce local biases (e.g., with state-of-the-art geophysical corrections or multi-mission calibration) or help better remove artifacts that might otherwise alter mesoscale statistics, SSHA derivatives, and their interpretation (e.g., editing or noise mitigation). For smaller scales and surface interactions, the 250 m Level-3 product (unsmoothed variant) assembles all the assets needed to explore the 250 m resolution conveniently (in comparison, the Level-2 unsmoothed product is technical but requires more specialized processing).

5.2 Tides

Fu et al. (2024) report how KaRIn's resolution and precision are a major breakthroughs in the analysis of barotropic and baroclinic tides (internal tides or IT). The barotropic part is relatively well-known in the open ocean, where recent tidal models such as FES or GOT are as precise as 5 mm rms. In contrast, the coverage of nadir altimeters is sparse and insufficient in regions of shallow bathymetry, in coastal seas, or in the high-latitude polar regions. Using KaRIn 250 m or 2 km products to improve barotropic tides requires good SSHA accuracy over scales ranging from a few tens of kilometers in coastal regions to thousands of kilometers for the continental shelf to the open ocean.

In that context, an important limiting factor is the KaRIn calibration process. The uncalibrated KaRIn images (see Fig. 3) can be skewed by tens of centimeters (residual error in the satellite attitude determination) across or along-track, which may be at similar scales to barotropic tides, so it is necessary to use a data-driven calibration mechanism, such as our Level-3 algorithm from Sect. 3.3 or the Level-2 counterpart. Since these calibration algorithms are data driven (i.e., empirical), they may also absorb some geophysical residuals as well (e.g., residuals after the FES22 model has been applied). This might be good for mesoscale users, since tides are generally considered an error by this community. However, tidal residuals are a signal for tides experts. Therefore, the L2/L3 calibration process may be partially detrimental for this community.

As the tides community starts analyzing longer time series of SWOT data, more in-depth analyses of the Level-2 and Level-3 calibrations are required in collaboration with them to quantify how this geophysical content might leak into the data-driven calibration corrections. This future collaborative analysis could lead to better calibration algorithms over the

ocean and improved tidal models in the key coastal, regional, and high-latitude regions.

The baroclinic tides have a very different paradigm. Although SWOT products have a baroclinic tidal model correction applied to reduce their signature in the SWOT SSHA, this model only captures the first mode (i.e., larger scales) of a few constituents, as well as only the stationary part of internal tides. KaRIn L3 data capture a vast range of baroclinic tide signatures that are not corrected by these models (Fig. 19). Panel (a) is a segment of SWOT measurements (altimeter and interferometer) in the North Atlantic. In the southern part of this region (right panel), there is smooth bathymetry, where the internal tides look like very regular wave trains every 12 h. Conversely, in the northern part of the scene (left panel), the bathymetry is rugged (mid-Atlantic rift), and the nature of the baroclinic internal tide (IT) surface topography changes: the KaRIn image looks like scrambled or random wave patterns.

Although modes 1 and 2 (i.e., more than 50 km) are present in both scenes, the striking features of KaRIn's observation are the smallest scales and nonlinear fraction of the waves: they aggregate into thin lines on the order of 10 km or less. This is the size of the SWOT nadir altimeter footprint. The SWOT nadir altimeter also has more random noise than KaRIn does. As a result, the altimeter does provide a consistent measurement of the internal tides in Fig. 19a, albeit a smoothed and noisy one. For this reason, current internal tidal models, which were built from 1D nadir altimetry, do not capture the full extent of the internal tide signal or its spatial structure. The residual is visible in all KaRIn SSHA products, including our Level-3 product.

Preliminary analyses of KaRIn-observed internal tides report that a substantial part of their variance is non-stationary (Tchilibou et al., 2024), so current IT models only capture a relatively small fraction of the variance that is observed by SWOT. However, the KaRIn breakthrough of 2D observation for baroclinic tides should lead to progress in their modeling and their correction in altimetry (1D and 2D).

Our current Level-3 processing might be affected by these IT residuals at different steps of the processing. The editing and noise mitigation might be confused by the smallest ripples of the baroclinic tide SSHA signature and try to flag/remove them. Moreover, when the propagation of internal waves is orthogonal to the satellite track (e.g., the circular wave in the right-hand-side zoom of Fig. 19a above a seamount), the apparent along-track wavelength might be long enough to leak into the data-driven calibration. This phenomenon was observed in the Bay of Bengal (not shown), where IT wave trains radiate from the eastern part of the basin (Andaman Islands): the SSHA exhibits very coherent wave signatures over more than 1000 km that are aliased at tidal frequencies. Similarly, in the Mascarene region (Fig. 19b), circular patterns are visible, are geographically coherent over very long distances, and are shifted but visible on neighboring tracks separated by some days. It is possible that a small fraction of this IT variance leaks into our data-driven calibration.

These findings have two consequences. Firstly, it could be important for baroclinic tide experts to explore how the Level-2 and Level-3 processing affects their signal of interest when they use SWOT measurement to develop new and better models. Secondly, it is clear that progress is needed on the IT model corrections for KaRIn, and SWOT is an excellent test bed for new models. More generally, the separation of balanced and unbalanced motion is extremely important to better interpret KaRIn images. As discussed in Sect. 3.1, our Level-3 processor can integrate state-of-the-art research-grade models for large-scale evaluation of these models beyond the expert tides community. In other words, our Level-3 framework is a good example of a sandbox product for testing new candidate tide algorithms and models before they are adopted by the community into the SWOT Level-2 ground segment.

5.3 High-frequency atmospheric effects

Like all nadir altimeters, SWOT products are corrected for various atmospheric effects: radar path delay in the atmosphere, inverse barometer effects, aliased barotropic response to wind and pressure forcing, etc. Most of these corrections are derived from weather models such as the European Centre for Medium-Range Weather Forecasts (ECMWF).

The KaRIn SSHA images sometimes highlight the limits of the atmospheric corrections, for instance in the presence of atmospheric lee waves (Fig. 20). These internal gravity waves of the atmosphere are caused by vertical air displacement after the wind flows over a mountain (here the island chains in the northwest part of the scene). On the downwind side of the terrain (the center of Fig. 20), they cause a periodic change in the pressure, wind, and atmospheric temperature fields, as well as wet-troposphere content. This is causing the wavelike patterns in panels (b) and (d) that did not exist the day before in panels (a) and (c). Each oscillation is on the order of 10 km, i.e., barely captured by a nadir altimeter but observed well by KaRIn. Such patterns are frequently observed in the sigma0 surface roughness fields of SAR images, and KaRIn captures the same changes in surface roughness with the periodic changes in the surface wind. KaRIn also shows the impact of these waves on the ocean surface topography.

These atmospheric features are below the spatial resolution of the Level-2 dynamic atmospheric correction (DAC) that are forced by ECMWF winds and pressure, as well as being smaller than the footprint of the SWOT microwave radiometer providing wet-troposphere corrections for KaRIn. In other words, the lee-wave signature in the KaRIn SSHA is very likely a measurement artifact caused by imperfect atmospheric corrections (e.g., inverse barometer, wet troposphere). These lee-wave features exist in many regions, although they might appear randomly depending on surface

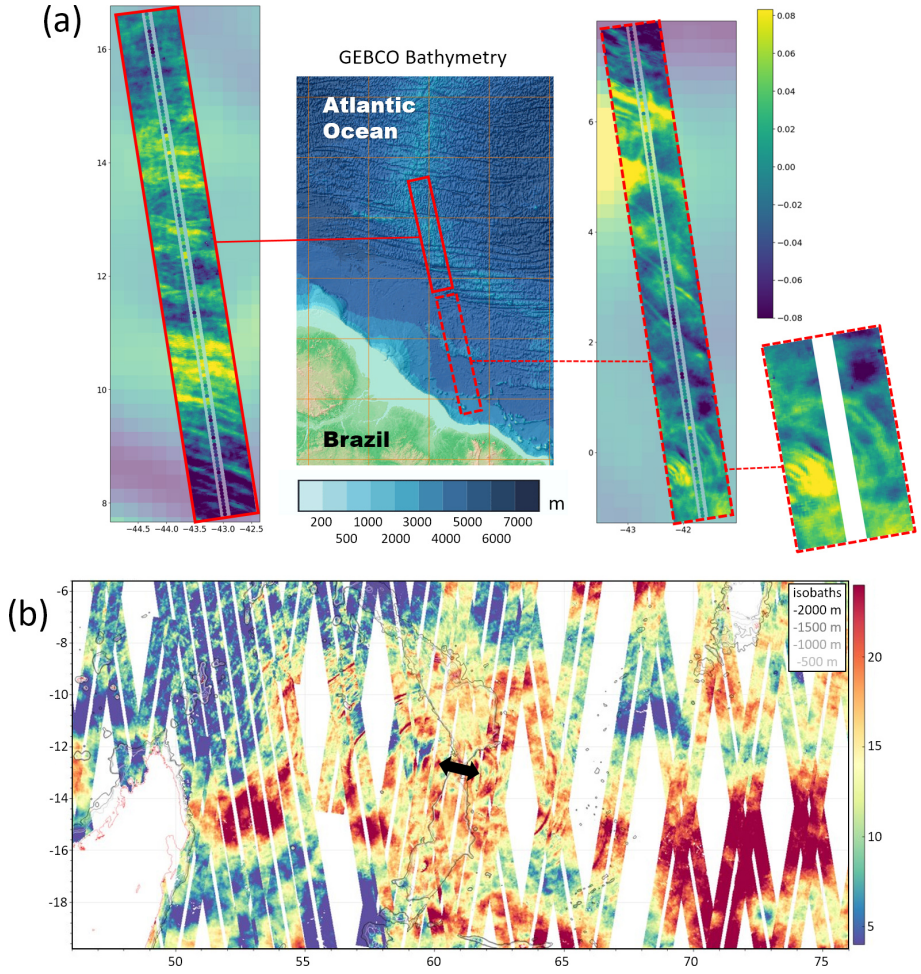

Figure 19. Signature of internal tides in the Level-3 product. Panel **(a)** is the KaRIn SSH (in cm) for the 1 d orbit in the North Atlantic Ocean, with a transition between smooth bathymetry (right-hand-side segment) and rugged bathymetry (left-hand-side segment). Panel **(b)** is the weekly coverage for the 21 d orbit over the Mascarene Plateau (isobaths in black) in the Indian Ocean. Circular internal tides are radiating from the gap (black arrow) between the Saya de Malha Bank and the Nazareth Bank.

wind conditions. This is an example of how the joint analysis of the SWOT-collocated SAR sigma0 images and SSHA can help us understand what might be actual small-scale ocean signals and what might be introduced by corrections that are not yet at the required resolution. These waves will be more frequent in the coastal zones or near islands, so user beware! Once again, the Level-3 product could serve as a sandbox demonstration for experimental higher-resolution atmospheric corrections (e.g., regional DAC based on a higher-resolution model).

Sometimes, KaRIn images can capture the rapid ocean response to extreme atmospheric signatures in the measured SSHA (Fig. 21). Indeed, Fig. 21a shows a series of six KaRIn daily images from the calibration phase, when SWOT sampled the same track daily. Here, SWOT crosses the trajectory of Cyclone Betty/Mawar in the tropical western Pacific: 3 d before the cyclone, during the cyclone itself, and 2 d after the cyclone. During the cyclone overflight, KaRIn measurements are strongly affected by the presence of heavy rain in the arms of the cyclone spiral[13]. In the 2 km product, the entire cyclone segment becomes very difficult to use. Conversely, the 250 m counterpart in Fig. 21b provides more ways to detect the rain regions (blue/red noise) and the regions without rain between the spiral arms (green/blue/yellow regions). In the eye of the cyclone, the sky is clear, and the topography is pulled higher than the rest of the scene by tens of centimeters. That is likely an inverse barometer response to the cyclone depression; i.e., it should be corrected for by the DAC correction. But the correction does not have the space and time resolution to resolve this extreme event.

The temporal evolution of the background ocean between the left and right panels of Fig. 21a (i.e., before/after the cyclone has crossed the KaRIn swath) shows a large, warm-

[13]In this example, we are not using the editing layer, as it would remove most of the scene.

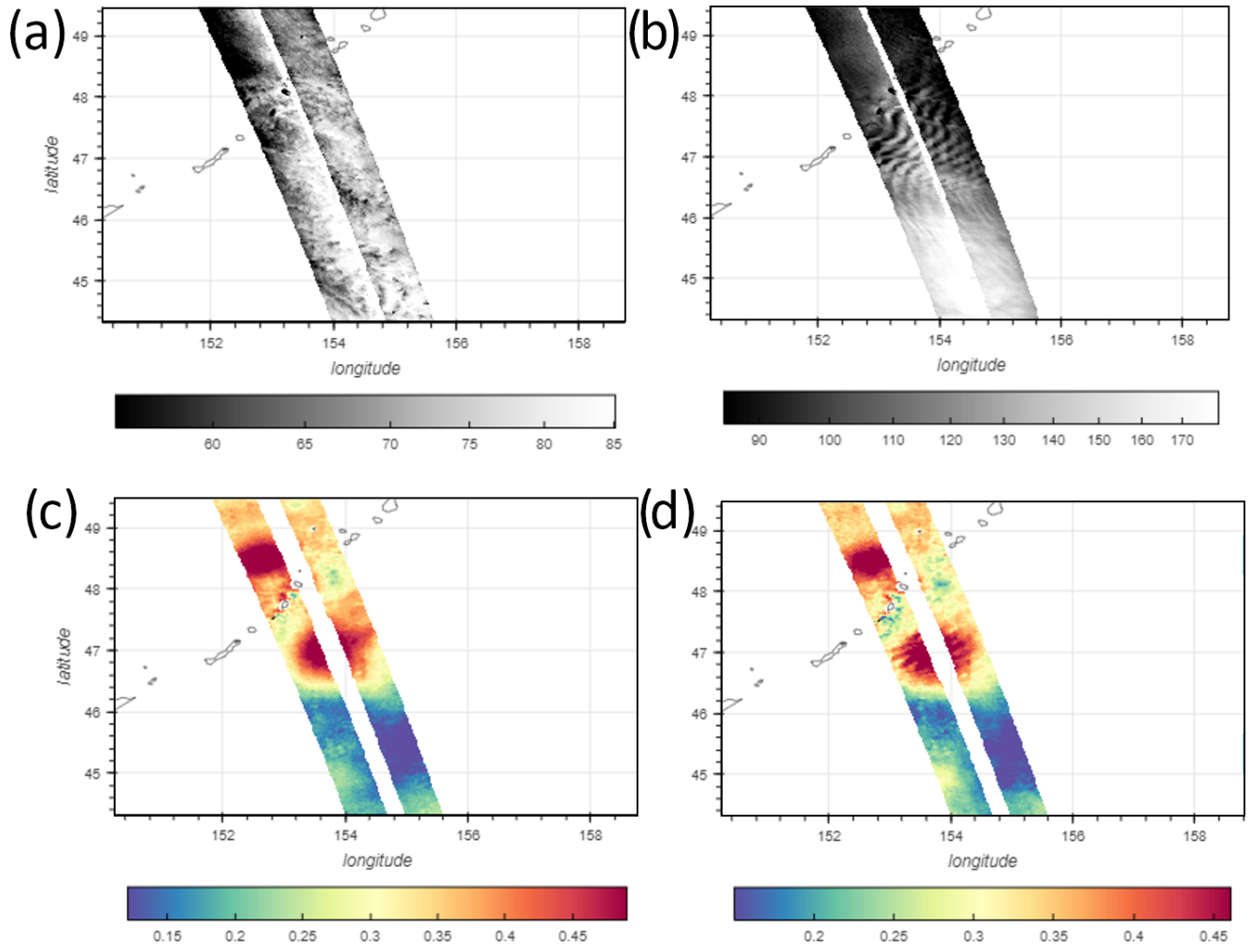

Figure 20. Example of SWOT Level-3 SSHAs over an atmospheric lee wave (Aleutian Islands, north Pacific Ocean). Panels **(a)** and **(b)** are the L2 sigma0 from KaRIn (linear), and panels **(c)** and **(d)** are the KaRIn SSHAs in meters. Panels **(a)** and **(c)** and panels **(b)** and **(d)** are 24 h apart.

mesoscale eddy developing before the cyclone, then the SSHA goes down by 20 cm or more (in only 2 d). This is a good example of how a tropical cyclone may siphon up the latent heat in the upper layers of the ocean and/or cause an adjustment in SSH (i.e., move the heat laterally). This example derived from our Level-3 product gives a very good 2D view of the event, including waves radiating from the cyclone when it is not yet or no longer within the SWOT swath.

Similarly, SWOT might be affected by the presence of intense wind fronts (Fig. 21c). In this 250 m Level-3 SSHA image, there is a sharp SSHA offset of 10 cm over less than 1 km along the storm front (the offset in wind speed is approximately 20 m s^{-1}). Looking at weather model is not particularly helpful, as the model hindcast predicts that the front is in a different position (it travels very quickly). In this example, it is not clear if the KaRIn SSHA offset is real, is caused by an SSH measurement artifact (e.g., lack of resolution of atmospheric path delay or sea-state bias), or is caused by a deficiency in the DAC correction. The nadir altimeter observes the offset, but it is noisier and spread out due to the larger altimeter footprint.

This large frontal offset of 10 cm associated with the wind front could affect some Level-3 algorithms and in particular the Level-3 empirical calibration: the calibration could interpret the offset as a KaRIn systematic error (bias term B or cross-track slope term L) and in turn create calibration artifacts over thousands of kilometers along this specific pass. Due to the magnitude of 10 cm, even a small leakage might be large enough to affect validation metrics.

Exploring these topics is not simple: it requires many different skill sets (e.g., remote sensing, atmosphere modeling, sea-state modeling, data-driven calibration,). Still, from these examples, it is clear that updating atmospheric corrections

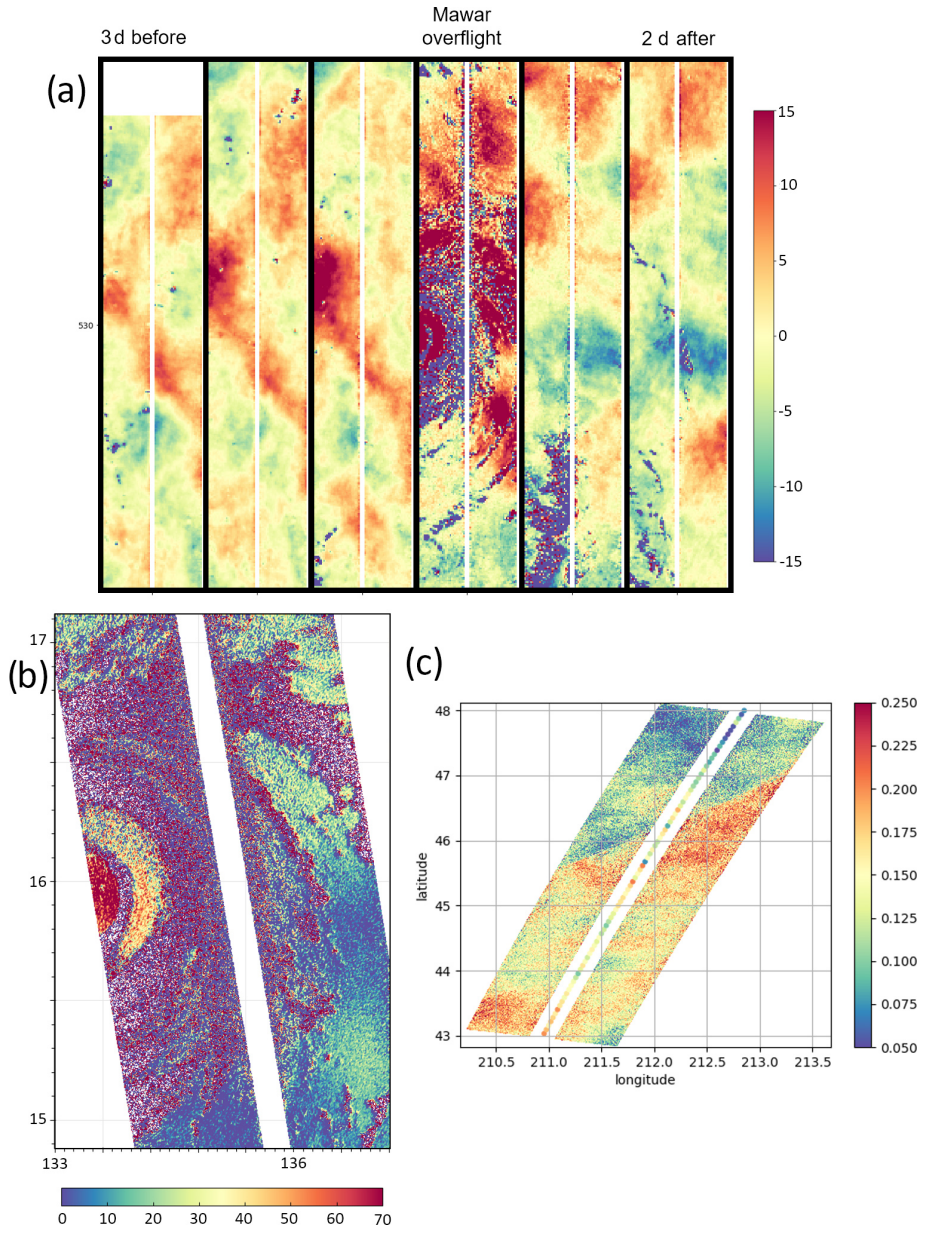

Figure 21. KaRIn Level-3 topography when SWOT crosses the trajectory of Cyclone Mawar/Betty in the western Pacific Ocean during the 1 d phase of SWOT. Panel **(a)** is a time series of 6 subsequent days in the same region (3 d before the cyclone and 2 d after the cyclone). Panel **(b)** is the cyclone overflight seen at 250 m resolution (in cm). Panel **(c)** is an example of 250 m SSHA (in m) when SWOT crosses an intense wind front (here 20 m s^{-1}) in the north Pacific Ocean (cycle 2, pass 41).

with research-grade models might interact with Level-3 algorithms.

5.4 Coastal regions

Coastal regions are known to be challenging for nadir altimetry (Vignudelli et al., 2019). The radius of their footprint is often a limiting factor: land can contaminate the altimeter waveform and create various artifacts, which may randomly affect all the retracked parameters. In contrast, SAR interferometry can extend up to land, and Fig. 22 illustrates how 250 m KaRIn measurements provide a seamless SSHA transition from the open ocean to the continental string of islands and then to coastal regions. These maps cover the Black Point district in the Bahamas, with very sharp transitions between deep waters (2000 m or more,; dark blue in panel a) to very shallow waters (20 to 30 m; cyan to white in panel a) up to the long island chain in the middle of the scene.

This region has complex circulation patterns, as well as complex wave generation/propagation due to the bathymetry.

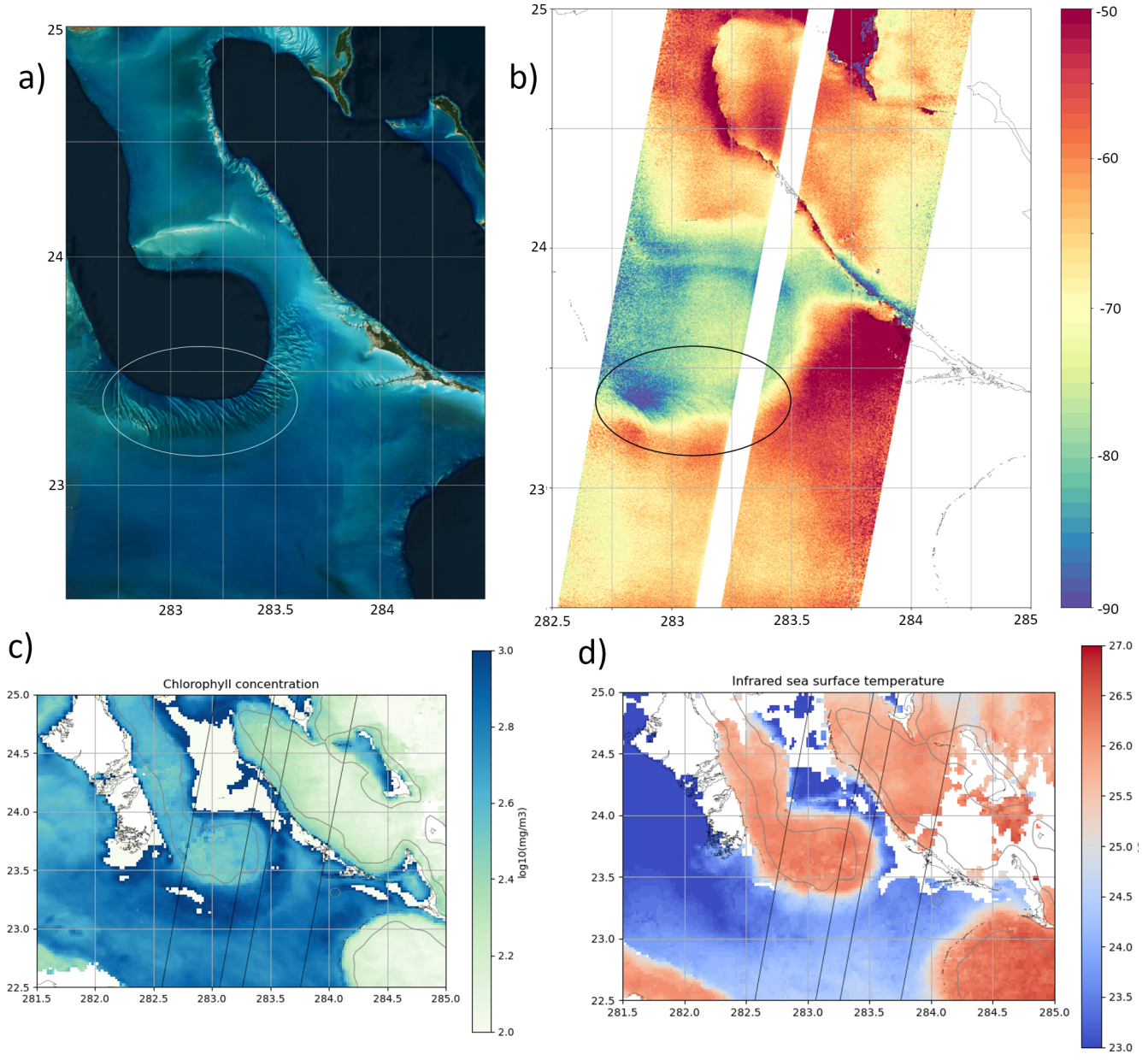

Figure 22. Overview of the SWOT measurements at the Black Point district in the Bahamas. Panel **(a)** is ESRI optical imagery: dark-blue regions have a bathymetry of 2000 m or more, and cyan-to-white regions are shallow waters of the order of tens of meters. Panel **(b)** is the 250 m KaRIn SSHA (in cm). Panels **(b)** and **(c)** are ocean color and sea surface temperature maps from Copernicus Marine Service.

Contrary to the sparse coverage of nadir altimeters (e.g., a Jason-class mission would provide 2×1D lines every 10 d in this scene), KaRIn captures this complexity with an unprecedented wealth of coverage and precision. In this specific image, KaRIn's 250 m noise is barely noticeable due to low-wave conditions, and KaRIn observes the deep-water-circulation patterns correlated with the bathymetry, with similar patterns in sea surface temperature and ocean color maps in panels (c) and (d). The 250 m SSHA also exhibits very thin lines that are aligned with the shallow underwater dunes of this region.

Importantly, the SSHA is defined up to the last coastal pixel, showing a clear discrepancy between the western and eastern sides of the island chain that is not observed by nadir altimeters (because of their measurement errors very close to the coast). It is very likely that the last few kilometers might be affected by the limited resolution of various geophysical models: the DAC model, the tidal models, and the MSS models are unlikely to resolve these kilometer-scale

or 250 m scale features since they are derived from lower-resolution nadir altimeter data from previous missions of the past decades.

These limitations cannot be resolved from one image; however an animated sequence of 90 KaRIn images during the 1 d phase of SWOT highlights that some patterns are time invariant (i.e., likely geoid error), while the island chain's regional bias is modulated at the tidal aliasing periods (i.e., likely tidal error). The shallow waters are also biased under specific pressure and wind conditions (i.e., DAC errors). New measurements from SWOT are limited by the resolution of these current models, but KaRIn is also (and by far) the best asset to improve the next generation of some geophysical models (e.g., tides, MSS, MDT).

In that context, our Level-3 unsmoothed 250 m variant tries to provide all the necessary elements for such expert investigations (e.g., each individual geophysical model that is not included in the 250 m Level-2 product) but does not include all the technical variables related to the instrument: it is a tradeoff between convenience for thematic studies and data volume. However, as discussed in the previous sections, it is likely that our editing or calibration procedures might be suboptimal in coastal transitions. More in-depth analyses by coastal and regional experts are needed to quantify the limitations, and a collaborative approach would likely make it possible to define good test beds for our algorithms or to propose improvements in geophysical models.

5.5 Hydrology

In their prelaunch assessments of the data-driven calibration, Dibarboure et al. (2017); Dibarboure and Ubelmann (2014) predicted that the ground segment Level-2 algorithm based on ocean crossovers could be insufficient to meet the requirements during the 1 d phase of the SWOT mission because there are very few crossover diamonds with SWOT alone. In that context, our Level-3 multi-mission calibration was initially designed as a backup algorithm able to meet the hydrology requirements. Conversely, for the 21 d phase, the crossover L2 algorithm and our multi-mission L3 algorithm were shown to have similar performance for hydrology, as the inland interpolation is the primary source of error.

Ubelmann et al. (2024) report that both predictions turned out to be true for the Level-2 version B (beta pre-validated). So our research-grade algorithm from Sect. 3.3 was adopted by the SWOT project as the default Level-2 algorithm for the 1 d phase of SWOT in their reprocessing, version C (winter 2024). In practice, we delivered the calibration parameters as a by-product of our Level-3 processor, and this correction was input from the SWOT project's Level-2 processor. Conversely, the single-mission L2 crossover calibration remains the default correction for the 21 d phase, as a SWOT standalone algorithm has simpler interfaces (no external satellite) than our research-grade processor and for a very similar output performance over hydrology surfaces.

In that context, our current Level-3 calibration is by no means optimal for hydrology, and various improvements could be added: better interpolators for inland or polar segments, better reduction in coastal variability (e.g., tides and DAC leakage into inland water heights), and adding inland reference points from stable targets (e.g., charted lakes and reservoirs, bridges, and roads). It is also likely that the optimal calibration algorithm for ocean/coastal/estuary users might be different from the optimal solution for inland rivers and lakes that are not in the tidal region. Exploring these differences in the future will require a wide set of skills from data-driven calibration, coastal ocean physics, hydrology physics, and in situ ground truth.

5.6 Polar regions and sea ice

KaRIn's 250 m resolution is generally not needed to study open-ocean mesoscale structures, but it becomes a powerful asset in polar regions covered by sea ice (Fig. 23). Indeed, the higher resolution makes it possible to retrieve the ocean surface topography in smaller polynyas and to retrieve surface ice/snow topography, as well as the difference between the ice/snow and ocean surface (sea-ice thickness in the freeboard region). Figure 23 is a composite between our 2 km basic Level-3 product in the Southern Ocean and our 250 m unsmoothed product in the polar regions. The zoom in panel (b) shows that our Level-3 calibration is generally decent (consistent color scheme for the ice topography) but not perfect in these regions: some passes have a bias of a few centimeters.

Moreover, the polynyas are easy to recognize from the image texture (Fig. 23c): water between the ice is visible as dark-blue pixels in the SSHA and as white pixels in the sigma0[14]. In panel (d), we use a simple and arbitrary sigma0 threshold to separate bright and dark pixels. The resulting topography PDF clearly shows two very different populations: the ice and snow PDF is bell-shaped, as expected from the terrain roughness, while the ocean PDF is very peaky and skewed. The difference between the median values of both distributions would suggest a difference of 15 cm between the surface of the ice/snow and the ocean.

This very simple example captures the potential of KaRIn's 250 m resolution, but it also illustrates how Level-3 algorithms are important for this type of analysis. Indeed, if the KaRIn topography is skewed by 5 to 10 cm (because of tidal model or data-driven calibration), it becomes extremely difficult to use an image like in Fig. 23d. Furthermore, Dibarboure et al. (2022) have shown that the Level-2 editing and calibration can be suboptimal in polar regions, especially during the wintertime, while the Level-3 version is substantially more robust. Similarly, the MSS and tidal models have various sources of errors in these regions. Therefore, any im-

[14]Note that when there is no wind or when the wind blows in a direction orthogonal to thin ice cracks, the water surface can be very dark rather than very bright. The dielectric constant of freezing water may also affect the sigma0 image.

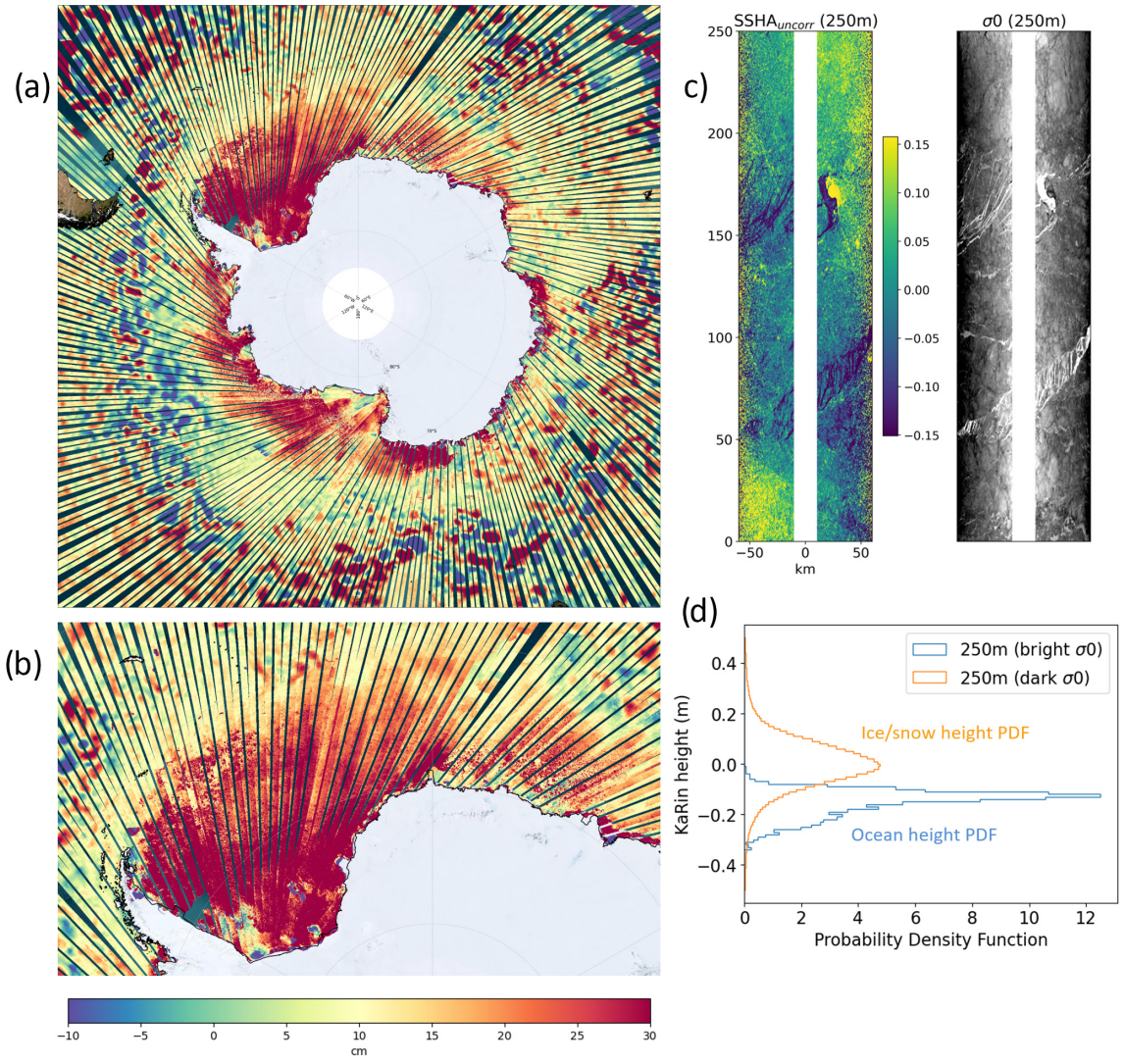

Figure 23. KaRIn SSHA in the southern polar region. Panel **(a)** maps the eddy field in the Antarctic Circumpolar Current and the sea-ice topography closer to Antarctica. Panel **(b)** is a zoom of the western part of the sea-ice coverage. Panel **(c)** is an arbitrary KaRIn segment over the sea ice. The 250 m KaRIn Level-3 SSHA (in cm) is on the left and the KaRIn Level-2 sigma0 (linear) is on the right. Panel **(d)** shows the height PDF for the bright and dark targets of panel **(c)** (arbitrary threshold on the sigma0 per pixel).

provements in research-grade geophysical models and calibration could make a difference for polar regions. Validating such improvements would only be possible with the help of experts from the polar community.

5.7 Future developments and collaborative Level-3 framework

SWOT and KaRIn demonstrate a breakthrough in the observation of surface water topography. Moreover, our Level-3 processor proves that one can integrate the new observing capabilities from SWOT into established altimetry multi-mission processors that have been operating for 3 decades. However, the current KaRIn algorithms and format are still not mature and will be progressively improved over time. This paper reports a series of Level-2 and Level-3 limitations (e.g., editing in coastal regions or suboptimal calibration in polar regions) that must be addressed in collaboration with various experts (from SWOT and other communities). It is likely that more limitations will be reported by external users and independent validation.

From the very different examples presented above, it is clear that improving SWOT products is not just the sum of independent corrections and algorithms. There are multiple and intertwined problems: sensor processing (nadir and KaRIn), Level-2 geophysical corrections, Level-3 processing layers, and regional or surface-specific dynamics that might leak into any item based on SSHA (e.g., empirical sea-state bias, tidal model with assimilation).

Therefore, it is clear that Level-3 algorithms cannot be developed and improved in a vacuum, with a single, homogeneous user community in mind. It is necessary to address thematic needs in tight collaboration with each user community, as well as in collaboration with ground segment algorithm experts.

In that context, our future developments will focus on three aspects.

We plan to develop and to contribute to open and fair evaluation frameworks for experimental algorithms and corrections (e.g., L2/L3 ocean data challenges[15]).

We plan to integrate new state-of-the-art candidates (from all sources for all algorithm layers) as sandbox or demonstration reprocessing. Our objective is to ease the SWOT product evaluation for users with pre-made and convenient-to-use products, as well as to investigate how a given algorithm improvement might be intertwined with other algorithm layers or specific needs from a given user community.

We plan to explore the possibility and relevance of replacing our one-size-fits-all L3 product with community-specific layers and products (e.g., hydrology, coastal, or polar ocean products). It is useful to have continuity from one surface to another, but the algorithms may need to be adapted and tuned differently.

Our current Level-3 product integrates state-of-the-art research from various research groups. We plan to keep integrating as many external contributions from the research community as possible, while keeping a flexible but consistent and comprehensive set of reprocessed products and near-real-time operations.

6 Summary and conclusions

Despite SWOT's unprecedented 2D coverage and precision, the Level-2 products suffer from the same limitations as similar products from other altimetry missions. They were designed in a standalone framework to meet the mission's primary science objective. In contrast, some research topics and applications require consistent multi-mission products, such as the Level-3 products provided by the Data Unification and Altimeter Combination System (DUACS) for almost 3 decades and using 20 different satellites.

In this paper, we describe how we extended the Level-3 algorithms to handle SWOT's unique swath-altimeter data: upgrades to state-of-the-art Level-2 corrections and models from the research community, a data-driven and statistical approach to the removal of spurious and suspicious pixels, a multi-satellite calibration process that leverages the strengths of the pre-existing nadir altimeter constellation, and merging of the 1D nadir altimeter and 2D interferometer from SWOT into a single product. Our qualitative comparisons with other sensors and quantitative comparisons with external nadir altimeters illustrate the strengths of SWOT/KaRIn and the consistency with other satellites.

We also illustrate and discuss the benefits and relevance of Level-3 swath-altimeter products for various research domains: basin-scale features (e.g., as large as El Niño), global circulation and ocean mesoscale (from tens to hundreds of kilometers), tides and atmospheric studies, and coastal and polar regions. Our Level-3 basic and unsmoothed products are more compact and are arguably simpler to use than their Level-2 counterparts, while the Level-3 expert variant give more flexibility and control to those who want to customize it.

More importantly, we illustrate how some data-driven algorithms and models from SWOT may create complex intertwined problems in a ground-breaking instrument such as KaRIn: leveraging the full potential of 2D images requires a diverse set of skills but also a consistent multi-mission and multi-thematic strategy. This has been a strong asset of the Data Unification and Altimeter Combination System (DUACS). Our current Level-3 swath processor was developed and is now extending this capability to SWOT to find a good tradeoff between continuously evolving state-of-the-art models, corrections and processing techniques, and consistent reprocessing of past data and forward near-real-time products.

Appendix A: Input data and standards

At the time of this writing, the Level-3 product is available in two releases: version 0.3 was made public on AVISO in December 2023 (see "Data availability" section), and version 1.0 was released in May 2024. The objective of this appendix is to give more details about the contents and the differences between them.

Firstly, the input Level-2 products are different. This point is illustrated by Fig. A1:

- L3 version 0.3 is based on the Level-2 version B, also known as PIB0 or beta pre-validated. The term pre-validated refers to the SWOT project timeline: the validation phase of the satellite spans spring 2023 to spring 2024, and the project managers had planned an interim or pre-validated product for public evaluation before the end of the validation phase. The beta term refers to the fact that SWOT products were deemed good enough and distributed a few months ahead of schedule, albeit with known and documented limitations from the ground segment. Our Level-3 product v0.3 inherits these beta limitations. It also has its own imperfections from the first generation of Level-3 algorithms.

- L3 version 1.0 is based on the Level-2 version C, also known as PIC0 for near real time and PGC0 for reprocessed data. This is the official pre-validated (not beta)

[15] https://github.com/ocean-data-challenges (last access: 12 November 2024)

product[16]. The Level-3 v1.0 product naturally inherits these ground segment upgrades. Similarly, the reprocessed periods in Fig. A1 benefit from a few parameters that were improved/reprocessed between PIC0 and PGC0 (see Table A1).

Lastly, various upgrades to the Level-3 algorithms were also added from v0.3 to v1.0 (this paper describes the 1.0 algorithms):

- We have upgraded the editing layers, added new algorithms for finer outlier detections (more layers and intermediate flag values), and added granularity and flexibility to the editing flags. In essence, this change now makes it possible for the user to control a more comprehensive L3 editing process from the expert variant (otherwise, the basic L3 product is still a good default starting point).
- We have upgraded the phase screen correction to better mitigate small-scale semi-static calibration residuals on the order of a few millimeters. This should be transparent for most oceanographers but is a good addition for geodesists and for all users to whom where millimeter-scale systematic biases are relevant.
- We have improved the L3 calibration mechanism to reconcile the L2 and L3 calibrations: one bias from KaRIn in the SWOT nadir altimeter and one bias from SWOT in the rest of the nadir constellation and in Sentinel-6. We have also added a new quality flag for the L3 calibration to isolate outliers and suspicious segments for this algorithm.
- We have retrained the noise-reduction UNet for better and more stable performance (retraining, new ocean models with tides, style transfer for measurement errors). Version 1.0 should have fewer artifacts than v0.3.
- We have tweaked the L3 format to make it more compatible with various standards and generic libraries and tools.

[16]Since the release of the Level-2 product version C, the SWOT project has fixed some of the known pre-validated issues. The ground processor upgrade will culminate in the release of a Level-2 version D, as well as a full-mission reprocessing. While these matters will become obsolete in the future, it is currently relevant for L3 users of version 0.3 and 1.0 to check out the public L2 documentation for known limitations and weaknesses.

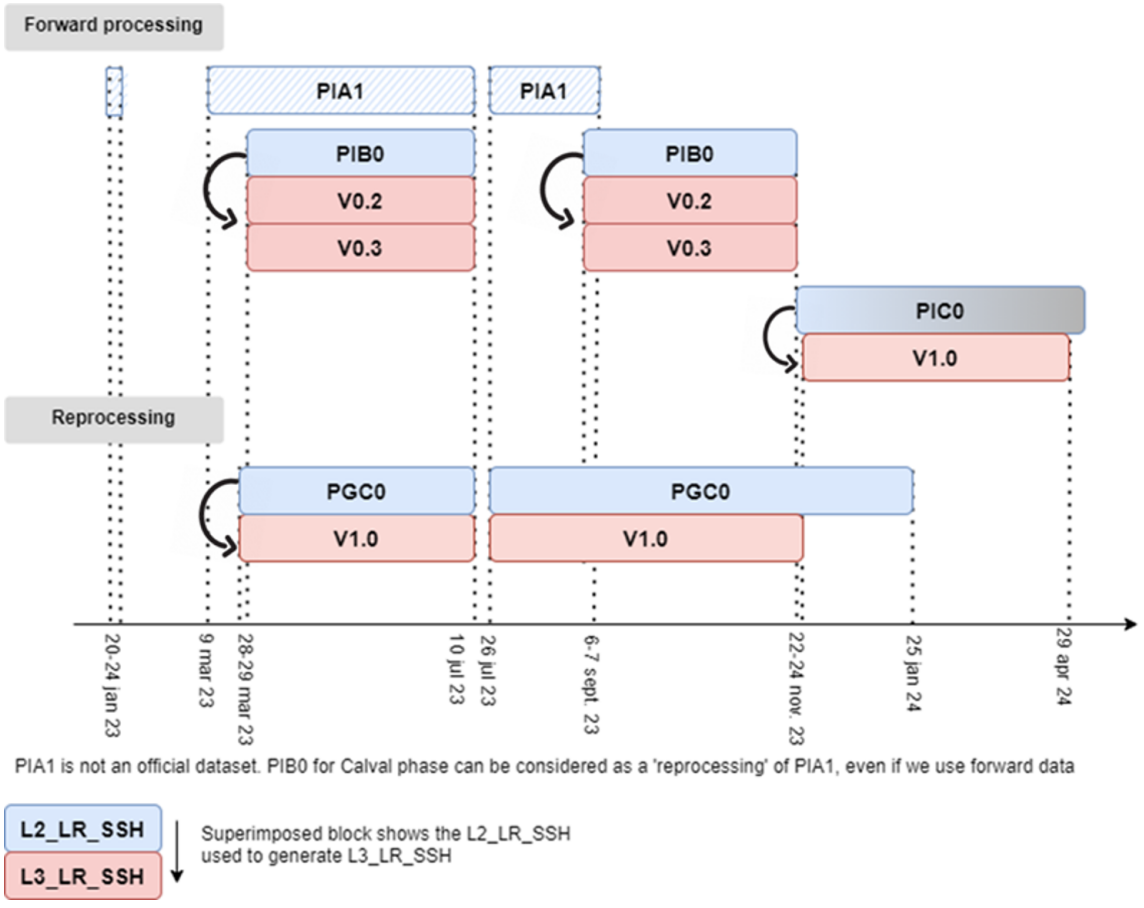

Figure A1. Schematics of the Level-2 and Level-3 product versions and their temporal coverage at the time of this writing. The blue boxes are the Level-2 products from the SWOT project, and the red boxes are our corresponding Level-3 products.

Table A1. Input data and altimeter standards used in the L3 KaRIn processor. Items in bold are specific to the L3 product. Other items are inherited from the L2 product.

	Level-3 product v0.3	Level-3 product v1.0
Input Level-2 product	PIA1 before 6 September 2023 PIB0 between 6 September and 23 November 2023 PIC0 after 23 November 2023	PGC0 before 23 November 2023 PIC0 after 23 November 2023
Orbit	MOE-F	POE-F until 30 April 2023 MOE-F after 30 April 2023
Ionosphere	NRT GIM model computed from vertical total electron content maps rescaled on the orbital altitude with the IRI95 model	GIM model computed from vertical total electron content maps rescaled on the orbital altitude with the IRI95 model (https://irimodel.org/, last access: 12 November 2024)
Wet troposphere	Model computed from ECMWF Gaussian grids	Model computed from ECMWF Gaussian grids
Sea state bias (SSB)	Non-parametric SSB from AltiKa GDR-F	Non-parametric SSB from AltiKa GDR-F
Mean profile/mean sea surface	**Hybrid MSS (SIO22, CNES/CLS22, DTU21) (Schaeffer et al., 2023; Laloue et al., 2025)**	**Hybrid MSS (SIO22, CNES/CLS22, DTU21) (Schaeffer et al., 2023; Laloue et al., 2025)**
Mean dynamic topography	**MDT CNES_CLS_2022 (Jousset and Mulet, 2020; Jousset et al., 2023)**	**MDT CNES_CLS_2022 (Jousset et Mulet, 2020; Jousset et al., 2023)**
Dry troposphere	Model computed from ECMWF Gaussian grids (new S1 and S2 atmospheric tides are applied)	Model computed from ECMWF Gaussian grids (new S1 and S2 atmospheric tides are applied)
DAC v4.0	TUGO forced with ECMWF pressure and wing fields (S1 and S2 were excluded), with the inverse barometer computed from rectangular grids	TUGO forced with ECMWF pressure and wing fields (S1 and S2 were excluded), with inverse barometer computed from rectangular grids
Ocean tide	**FES2022 (Lyard et al., 2025; Carrère et al., 2023)**	**FES2022 (Lyard et al., 2025; Carrère et al., 2023)**
Internal tide	HRETv8.1 tidal frequencies: M2, K1, S2, and O1	HRETv8.1 tidal frequencies: M2, K1, S2, and O1
Pole tide	mean pole location	mean pole location
Solid Earth tide	Elastic response to tidal potential	Elastic response to tidal potential
Loading tide	FES2022	FES2022

Data availability. All datasets discussed in this paper are preserved and distributed by the agencies' data repositories in compliance with FAIR requirements (e.g., a core trust seal (https://www.coretrustseal.org/, last access: 15 January 2025) certification, or ongoing certification from the Research Data Alliance (https://www.rd-alliance.org/, last access: 15 January 2025)).

- The Level-3 SWOT products generated in the framework of this study are distributed by the AVISO repository from CNES from the following DOIs:
  - L3 basic variant – https://doi.org/10.24400/527896/A01-2023.017 (AVISO/DUACS, 2024a).
  - L3 expert variant – https://doi.org/10.24400/527896/A01-2023.018 (AVISO/DUACS, 2024b).
  - L3 unsmoothed variant – https://doi.org/10.24400/527896/A01-2024.003 (AVISO/DUACS, 2024c).
- The SWOT products used in the paper are distributed by mirror centers from NASA and CNES. The SWOT products can be downloaded from either repository. Each SWOT product has a specific product description document (PDD) and digital object identifier (DOI):
  - NASA – https://podaac.jpl.nasa.gov/swot?tab=datasets (NASA, 2025) is the PODAAC repository for both ocean and hydrology products.
  - CNES – https://doi.org/10.24400/527896/A01-2023.016 (SWOT project, 2023a) is the AVISO repository for ocean products.
- Among the variety of SWOT Level-2 products available in the repositories, this paper specifically uses two products:
  - The SWOT Level 2 KaRIn low-rate sea surface height data product, version 1.1, is available from the two centers with two DOIs (https://doi.org/10.24400/527896/A01-2023.015 (SWOT project, 2023b) (AVISO, beta pre-validated collection) or https://doi.org/10.5067/SWOT-SSH-1.1 (SWOT, 2023) (PODAAC, collection ID SWOT_L2_LR_SSH_1.1)).
  - The SWOT Level-2 nadir altimeter data product (AVISO, collection L2_NALT_IGDR) is available from the following DOI: https://doi.org/10.24400/527896/a01-2023.005 (SWOT project, 2023c).
- This paper also uses Level-3 products from other altimetry missions (namely Sentinel-3, Jason-3, SARAL), as well as Level-4 gridded products, other nadir altimetry satellites, sea surface temperature, and sea surface chlorophyll concentration. These datasets are distributed by the Copernicus Marine Service repository: https://marine.copernicus.eu/access-data (last access: 12 November 2024).
  - The Level-3 along-track product is the SEALEVEL_GLO_PHY_L3_MY_008_062 product ID and is available from the following DOI: https://doi.org/10.48670/moi-00146 (CMEMS, 2024a).
  - The Level-4 gridded product is the SEALEVEL_GLO_PHY_L4_MY_008_047 product ID and is available from the following DOI: https://doi.org/10.48670/moi-00148 (CMEMS, 2024b).
  - The chlorophyll concentration is the OCEANCOLOUR_GLO_BGC_L3_NRT_009_101 product ID and is available from the following DOI: https://doi.org/10.48670/moi-00278 (CMEMS, 2024c).

Author contributions. Conceptualization – GD, CU, YF, and RM. Data curation – PP, EC, MR, FB, RC, and CA. Formal analysis – GD, PP, MR, MP, CA, and AT. Funding acquisition – GD and NP. Investigation – GD, RM, PP, CU, and MIP. Methodology – GD, RM, and YF. Project administration – GD, YF, and NP. Resources – FB, AD, RC, and AT. Software – FB, RC, and AD. Supervision – RM, GD, and YF. Validation – MIP, AD, PP, and CU. Visualization – AD, GD, YF, AT, and CU. Writing – GD, RM, YF, and MIP.

Competing interests. The contact author has declared that none of the authors has any competing interests.

Disclaimer. Publisher's note: Copernicus Publications remains neutral with regard to jurisdictional claims made in the text, published maps, institutional affiliations, or any other geographical representation in this paper. While Copernicus Publications makes every effort to include appropriate place names, the final responsibility lies with the authors.

Acknowledgements. The authors would like to thank the SWOT project from CNES and JPL/NASA for active help in accelerating the L3 operations during the SWOT adopt-a-crossover (https://www.swot-adac.org/, last access: 12 November 2024) validation campaigns, as well as thank the many members of the SWOT science team for their insights, evaluations, and feedback on the first alpha and beta L3 releases.

Financial support. This work was funded by the French Programme d'Investissement d'Avenir (https://www.gouvernement.fr/actualite/le-programme-d-investissements-d-avenir, last access: 12 November 2024) to accelerate the adoption of SWOT by the user community, as well as the development of SWOT downstream applications.

Review statement. This paper was edited by Bernadette Sloyan and reviewed by Tom Farrar and one anonymous referee.

References

Ajayi, A., Le Sommer, J., Chassignet, E., Molines, J.-M., Xu, X., Albert, A., and Cosme, E.: Spatial and Temporal Variability of the North Atlantic Eddy Field From Two Kilometric-Resolution Ocean Models, J. Geophys. Res.-Oceans, 125, e2019JC015827, https://doi.org/10.1029/2019JC015827, 2020.

Arbic, B. K., Scott, R. B., Chelton, D. B., Richman, J. G., and Shriver, J. F.: Effects of stencil width on surface ocean

geostrophic velocity and vorticity estimation from gridded satellite altimeter data, J. Geophys. Res.-Oceans, 117, C03029, https://doi.org/10.1029/2011JC007367, 2012.

AVISO/DUACS: SWOT Level-3 KaRIn Low Rate SSH Basic (v1.0.2), CNES [data set], https://doi.org/10.24400/527896/A01-2023.017, 2024a.

AVISO/DUACS: SWOT Level-3 KaRIn Low Rate SSH Expert (v1.0.2), CNES [data set], https://doi.org/10.24400/527896/A01-2023.018, 2024b.

AVISO/DUACS: SWOT Level-3 KaRIn Low Rate SSH Unsmoothed (v1.0.2), CNES [data set], https://doi.org/10.24400/527896/A01-2024.003, 2024c.

Ballarotta, M., Ubelmann, C., Pujol, M.-I., Taburet, G., Fournier, F., Legeais, J.-F., Faugère, Y., Delepoulle, A., Chelton, D., Dibarboure, G., and Picot, N.: On the resolutions of ocean altimetry maps, Ocean Sci., 15, 1091–1109, https://doi.org/10.5194/os-15-1091-2019, 2019.

Bohé, A.: KaRIn LR Oceanography Products Status & Examples, in: 2023 SWOT Science Team meeting, Toulouse, France, 2023, https://swotst.aviso.altimetry.fr/fileadmin/user_upload/SWOTST2023/20230919_2_Karin_overview1/11h30-BOHE_plenary.pdf (last access: 12 March 2024), 2023.

Brodeau, L., Sommer, J. L., and Albert, A.: ocean-next/eNATL60: Material describing the set-up and the assessment of NEMO-eNATL60 simulations, Zenodo [data set], https://doi.org/10.5281/zenodo.4032732, 2020.

Carrère, L., Lyard, F., Cancet, M., Allain, D., Fouchet, E., Dabat, M., Tchilibou, M., Ferrari, R., and Faugere, Y.: The new FES2022 Tidal atlas, in: 2023 SWOT Science Team meeting, Toulouse, France, 2023, https://doi.org/10.24400/527896/a03-2022.3287, 2023.

CEOS: The Next 15 Years of Satellite Altimetry Ocean Surface Topography Constellation: User Requirements Document, https://ceos.org/observations/documents/Satellite_Altimetry_Report_2009-10.pdf (last access: 12 March 2024), 2009.

Chelton, D. B., Samelson, R. M., and Farrar, J. T.: The effects of uncorrelated measurement noise on SWOT estimates of Sea surface height, velocity, and vorticity, J. Atmos. Ocean. Tech., 39, 1053–1083, 2022.

Chen, C.: Features of KaRIn Data that Users Should be Aware of, in: 2023 SWOT Science Team meeting, Toulouse, France, 2023, https://swotst.aviso.altimetry.fr/fileadmin/user_upload/SWOTST2023/20230919_3_Karin_overview2/14h10-KaRInFeatures.pdf (last access: 12 March 2024), 2023.

Davidson, F., Alvera-Azcarate, A., Barth, A., Brassington, G. B., Chassignet, E. P., Clementi, E., and Zu, Z.: Synergies in operational oceanography: the intrinsic need for sustained ocean observations, Front. Mar. Sci., 6, 450, https://doi.org/10.3389/fmars.2019.00450, 2019.

Dibarboure, G. and Morrow, R.: Value of the Jason-1 geodetic phase to study rapid oceanic changes and importance for defining a Jason-2 geodetic orbit, J. Atmos. Ocean. Tech., 33, 1913–1930, 2016.

Dibarboure, G. and Pujol, M. I.: Improving the quality of Sentinel-3A data with a hybrid mean sea surface model, and implications for Sentinel-3B and SWOT, Adv. Space Res., 68, 1116–1139, 2021.

Dibarboure, G. and Ubelmann, C.: Investigating the performance of four empirical cross-calibration methods for the proposed SWOT mission, Remote Sensing, 6, 4831–4869, 2014.

Dibarboure, G., Pujol, M.-I., Briol, F., Le Traon, P-Y., Larnicol, G., Picot, N., Mertz, F., and Ablain, M.: Jason-2 in DUACS: Updated System Description, First Tandem Results and Impact on Processing and Products, Mar. Geodesy, 34, 214–241, 2011.

Dibarboure, G., Ubelmann, C., Flamant, B., Briol, F., Peral, E., Bracher, G., and Picot, N.: Data-driven calibration algorithm and pre-launch performance simulations for the swot mission, Remote Sens., 14, 6070, https://doi.org/10.3390/rs14236070, 2022.

E.U. Copernicus Marine Service Information (CMEMS): Global Ocean Along Track L3 Sea Surface Heights Reprocessed 1993 Ongoing Tailored For Data Assimilation, E.U Copernicus Marine Service Information (CMEMS), Marine Data Store (MDS) [data set], https://doi.org/10.48670/moi-00146, 2024a.

E.U. Copernicus Marine Service Information (CMEMS): Global Ocean Gridded L4 Sea Surface Heights And Derived Variables Reprocessed 1993 Ongoing, E.U Copernicus Marine Service Information (CMEMS), Marine Data Store (MDS) [data set], https://doi.org/10.48670/moi-00148, 2024b.

E.U. Copernicus Marine Service Information (CMEMS): Global Ocean Colour (Copernicus-GlobColour), Bio-Geo-Chemical, L3 (daily) from Satellite Observations (Near Real Time), E.U Copernicus Marine Service Information (CMEMS), Marine Data Store (MDS) [data set], https://doi.org/10.48670/moi-00278, 2024c.

Faugère, Y., Taburet, G., Ballarotta, M., Pujol, I., Legeais, J. F., Maillard, G., Durand, C., Dagneau, Q., Lievin, M., Sanchez Roman, A., and Dibarboure, G.: DUACS DT2021: 28 years of reprocessed sea level altimetry products, EGU General Assembly 2022, Vienna, Austria, 23–27 May 2022, EGU22-7479, https://doi.org/10.5194/egusphere-egu22-7479, 2022.

Fjörtoft, R.: KaRIn HR Hydrology Products Status and Examples, in: 2023 SWOT Science Team meeting, Toulouse, France, 2023, https://swotst.aviso.altimetry.fr/fileadmin/user_upload/SWOTST2023/20230919_2_Karin_overview1/12h00-HR_Products.pdf (last access: 12 March 2024), 2023.

Fu, L.-L. and Rodriguez, E.: High-Resolution Measurement of Ocean Surface Topography by Radar Interferometry for Oceanographic and Geophysical Applications, in: The State of the Planet: Frontiers and Challenges in Geophysics, Geophys. Monogr. Ser., vol. 150, edited by: Sparks, R. S. J. and Hawkesworth, C. J., 209–224, https://doi.org/10.1029/150GM17, 2004.

Fu, L.-L., Pavelsky, T., Cretaux, J. F., Morrow, R., Farrar, J. T., Vaze, P., Sengenes, P., Vinogradova-Shiffer, N., Sylvestre-Baron, A., Picot, N., and Dibarboure, G.: The Surface Water and Ocean Topography Mission: A breakthrough in radar remote sensing of the ocean and land surface water, Geophys. Res. Lett., 51, e2023GL107652. https://doi.org/10.1029/2023GL107652, 2024.

Gatys, L. A., Ecker, A. S., and Bethge, M.: Image style transfer using convolutional neural networks, in: Proceedings of the IEEE conference on computer vision and pattern recognition, Las Vegas, NV, USA, 2016, 2414–2423, https://doi.org/10.1109/CVPR.2016.265, 2016.

Gómez-Navarro, L., Cosme, E., Sommer, J., Papadakis, N., and Pascual, A.: Development of an Image De-Noising Method in Preparation for the Surface Water and Ocean

Topography Satellite Mission, Remote Sens., 12, 734, https://doi.org/10.3390/rs12040734, 2020.

International Altimetry Team: Altimetry for the future: Building on 25 years of progress, Adv. Space Res., 68, 319–363, https://doi.org/10.1016/j.asr.2021.01.022, 2021.

Jousset, S. and Mulet, S.: New Mean Dynamic Topography of the Black Sea and Mediterranean Sea from altimetry, gravity and in-situ data, in: Presentation Ocean Surface Topography Science Team (OSTST), https://meetings.aviso.altimetry.fr/fileadmin/user_upload/tx_ausyclsseminar/files/OSTST2020_JOUSSET_MULET_MDT.pdf (last access: 15 January 2025), 2020.

Jousset, S., Mulet, S., Greiner, E., Wilkin, J. Vidar, L., Dibarboure, G., and Picot, N.: New Global Mean Dynamic Topography CNES-CLS-22 Combining Drifters, Hydrological Profiles and High Frequency Radar Data, ESS Open Archive, https://doi.org/10.22541/essoar.170158328.85804859/v1, 2023.

Kocha, C., Pageot, Y., Rubin, C., Lievin, M ., Pujol, M.-I., Philipps, S., Prandi, P., Labroue, S., Denis, I., Dibarboure, G., and Nogueira-Loddo, C.: 30 years of sea level anomaly reprocessed to improve climate and mesoscale satellite data record, in: 2023 Ocean Surface Topography Science Team meeting, https://doi.org/10.24400/527896/a03-2023.3805, 2023.

Laloue, A., Schaeffer, P., Pujol, M.-I., Veillard, P., Andersen, O., Sandwell, D., Delepoulle, A., Dibarboure, G., and Faugère, Y.: Merging recent Mean Sea Surface into a 2023 Hybrid model (from Scripps, DTU, CLS and CNES), in press, https://doi.org/10.22541/au.171987154.42384510/v1, 2025.

Lamy, A. and Albouys, V.: Mission design for the SWOT mission, in: Proceedings of the 2014 International Symposium on Space Flight Dynamics (ISSFD) meeting, Laurel, Maryland, USA, 5–9 May 2014, https://issfd.org/ISSFD_2014/ISSFD24_Paper_S17-1_LAMY.pdf (last access: 12 March 2024), 2014.

Le Traon, P. Y., Reppucci, A., Alvarez Fanjul, E., et al.: From observation to information and users: The Copernicus Marine Service perspective, Front. Mar. Sci., 6, 234, https://doi.org/10.3389/fmars.2019.00234, 2019.

Lyard, F., Carrere, L., Fouchet, E., Cancet, M., Greenberg, D., Dibarboure, G., and Picot, N.: FES2022 a step towards a SWOT-compliant tidal correction, Submitted to J. Geophy. Res., in review, 2025.

Morrow, R., Fu, L. L., Ardhuin, F., Benkiran, M., Chapron, B., Cosme, E., d'Ovidio, F., Farrar, J. T., Gille, S. T., Lapeyre, G., Le Traon, P.-Y., Pascual, A., Ponte, A., Qiu, B., Rascle, N., Ubelmann, C., Wang, J., and Zaron, E. D.: Global observations of fine-scale ocean surface topography with the surface water and ocean topography (SWOT) mission, Front. Mar. Sci., 6, 232, https://doi.org/10.3389/fmars.2019.00232, 2019.

Nichol, J. E., Antonarakis, A. S., and Nazeer, M.: Monitoring the sea surface microlayer (SML) on sentinel images, Sci. Total Environ., 872, 162218, https://doi.org/10.1016/j.scitotenv.2023.162218, 2023.

NASA: Surface Water and Ocean Topography (SWOT), NASA [data set], https://podaac.jpl.nasa.gov/swot?tab=datasets, last access: 28 January 2025.

Peral, E., Esteban-Fernández, D., Rodríguez, E., McWatters, D., De Bleser, J. W., Ahmed, R., Chen, A., Somawardhana, R., Johnson, M, Jaruwatanadilok, S., Wu, X., Peters, K., Chen, C., Khayatian, B., Chen, J., Hodges, R., Boussalis, D., Stiles, B., and Srinivasan, K.: KaRIn, the Ka-Band Radar Interferometer of the SWOT Mission: Design and In-Flight Performance, IEEE T. Geosci. Remote, 62, 5214127, https://doi.org/10.1109/TGRS.2024.3405343, 2024.

Picard, B., Picot, N., Dibarboure, G., and Steunou, N.: Characterizing Rain Cells as Measured by a Ka-Band Nadir Radar Altimeter: First Results and Impact on Future Altimetry Missions, Remote Sens., 13, 4861, https://doi.org/10.3390/rs13234861, 2021.

Pujol, M.-I., Faugère, Y., Taburet, G., Dupuy, S., Pelloquin, C., Ablain, M., and Picot, N.: DUACS DT2014: the new multi-mission altimeter data set reprocessed over 20 years, Ocean Sci., 12, 1067–1090, https://doi.org/10.5194/os-12-1067-2016, 2016.

Pujol, M.-I., Schaeffer, P., Faugère, Y., Raynal, M., Dibarboure, G., and Picot, N.: Gauging the improvement of recent mean sea surface models: A new approach for identifying and quantifying their errors, J. Geophy. Res.-Oceans, 123, 5889–5911, 2018.

Pujol, M.-I., Dupuy, S., Vergara, O., Sánchez Román, A., Faugère, Y., Prandi, P., Dabat, M.-L., Dagneaux, Q., Lievin, M., Cadier, E., Dibarboure, G., and Picot, N.: Refining the Resolution of DUACS Along-Track Level-3 Sea Level Altimetry Products, Remote Sens., 15, 793, https://doi.org/10.3390/rs15030793, 2023.

Rascle, N., Chapron, B., Ponte, A., Ardhuin, F., and Klein, P.: Surface roughness imaging of currents shows divergence and strain in the wind direction, J. Phys. Oceanogr., 44, 2153–2163, 2014.

Raynal, M., Dibarboure, G., Bohé, A., Bignalet-Cazalet, F., Picot, N., Prandi, P., Cadier, E., Nencioli, F., Briol, F., Delepoulle, A., Flamant, B., Denneulin, M., Picard, B., Ubelmann, C., Chen, C., and Stiles, B.: SWOT Phase E1 Results: 21-d orbit early CalVal results over Ocean, in: 2023 SWOT Science Team meeting, Toulouse, France, 2023, https://swotst.aviso.altimetry.fr/fileadmin/user_upload/SWOTST2023/20230922_1_going_forward/09h10-RAYNAL_L2LR_CalVal_scienceOrbit.pdf (last access: 12 March 2024), 2023.

Schaeffer, P., Pujol, M.-I., Veillard, P., Faugere, Y., Dagneau, Q., Dibarboure, G., Picot, N., Sandwell, D., Yu, Y., Harper, H., Andersen, O., Abulaitijiang, A., Zhang, S., and Rose, S.-K.: The 2023 Hybrid Mean Sea Surface, in: 2023 SWOT Science Team meeting, Toulouse, France, 2023, https://swotst.aviso.altimetry.fr/fileadmin/user_upload/SWOTST2023/20230921_ocean_2_mss/10h00-1-SCHAEFFER_Hybrid_MSS.pdf (last access: 12 March 2024), 2023.

Surface Water Ocean Topography (SWOT): SWOT Level 2 KaRIn Low Rate Sea Surface Height Data Product, Version 1.1. Ver. 1.1. PO.DAAC, CA, USA [data set], https://doi.org/10.5067/SWOT-SSH-1.1, 2023.

Surface Water Ocean Topography (SWOT): Mission Performance and Error Budget, NASA/JPL Document, Reference: JPL D-79084, Jet Propulsion Laboratory, Pasadena, CA, USA, 2013, https://swot.jpl.nasa.gov/system/documents/files/2178_2178_SWOT_D-79084_v10Y_FINAL_REVA__06082017.pdf (last access: 12 March 2024), 2024.

SWOT project: SWOT Level-2 KaRIn Low Rate SSH Unsmoothed (v2.0), CNES [data set], https://doi.org/10.24400/527896/A01-2023.016, 2023a.

SWOT project: SWOT Level-2 KaRIn Low Rate SSH Expert (v2.0), CNES [data set], https://doi.org/10.24400/527896/A01-2023.015, 2023b.

SWOT project: GDR (Geophysical Data Records), CNES [data set], https://doi.org/10.24400/527896/a01-2023.005, 2023c.

Taburet, G., Sanchez-Roman, A., Ballarotta, M., Pujol, M.-I., Legeais, J.-F., Fournier, F., Faugere, Y., and Dibarboure, G.: DUACS DT2018: 25 years of reprocessed sea level altimetry products, Ocean Sci., 15, 1207–1224, https://doi.org/10.5194/os-15-1207-2019, 2019.

Tchilibou, M., Carrere, L., Lyard, F., Ubelmann, C., Dibarboure, G., Zaron, E. D., and Arbic, B. K.: Internal tides off the Amazon shelf in the western tropical Atlantic: Analysis of SWOT Cal/Val Mission Data, EGUsphere [preprint], https://doi.org/10.5194/egusphere-2024-1857, 2024.

Tréboutte, A., Carli, E., Ballarotta, M., Carpentier, B., Faugère, Y., and Dibarboure, G.: KaRIn Noise Reduction Using a Convolutional Neural Network for the SWOT Ocean Products, Remote Sens, 15, 2183, https://doi.org/10.3390/rs15082183, 2023.

Ubelmann, C., Dibarboure, G., and Dubois, P.: A cross-spectral approach to measure the error budget of the SWOT altimetry mission over the Ocean, J. Atmos. Ocean. Tech., 35, 845–857, 2018.

Ubelmann, C., Dibarboure, G., Delepoulle, A., Faugère, Y., Prandi, P., Vayre, M., Briol, F., Bracher, G., Cadier, E., and Picot, N.: Data-driven calibration of SWOT's systematic errors: first in-flight assessment, Remote Sens., 16, 3558, https://doi.org/10.3390/rs16193558, 2024.

Vignudelli, S., Birol, F., Benveniste, J., Fu, L-L., Picot, N., Raynal, M., and Roinard, H.: Satellite altimetry measurements of sea level in the coastal zone, Surv. Geophys., 40, 1319–1349, 2019.

Yu, Y., Sandwell, D. T., Dibarboure, G., Chen, C., and Wang, J.: Accuracy and resolution of SWOT altimetry: Foundation seamounts, Earth Space Sci., 11, e2024EA003581, https://doi.org/10.1029/2024EA003581, 2024.